Coupled climate-carbon cycle simulation of the Last Glacial Maximum atmospheric CO_2 decrease using a large ensemble of modern plausible parameter sets

Krista M.S. Kemppinen[1], Philip B. Holden[2], Neil R. Edwards[2], Andy Ridgwell[3,4], Andrew D. Friend[1]

[1]Department of Geography, University of Cambridge, Cambridge CB2 3EN, UK
[2]Environment, Earth and Ecosystem Sciences, The Open University, Milton Keynes, MK7 6AA, UK
[3]School of Geographical Sciences, Bristol University, Bristol BS8 1SS, UK
[4]Department of Earth Sciences, University of California, Riverside, California 92521, USA

Correspondence to: Krista M.S. Kemppinen (Krista.Kemppinen@asu.edu)

Abstract. During the Last Glacial Maximum (LGM), atmospheric CO_2 was around 90 ppmv lower than during the preindustrial period. The reasons for this decrease are most often elucidated through factorial experiments testing the impact of individual mechanisms. Due to uncertainty in our understanding of the real system, however, the different models used to conduct the experiments inevitably take on different parameter values, and different structures. In this paper, the objective therefore, is to take an uncertainty-based approach to investigating the LGM CO_2 drop by simulating it with a large ensemble of parameter sets, designed to allow for a wide range of large-scale feedback response strengths. Our aim is not to definitely explain the causes of the CO_2 drop but rather explore the range of possible responses. We find that the LGM CO_2 decrease tends to predominantly be associated with decreasing sea surface temperatures (SSTs), increasing sea ice area, a weakening of the Atlantic Meridional Overturning Circulation (AMOC), a strengthening of the Antarctic Bottom Water (AABW) cell in the Atlantic Ocean, a decreasing ocean biological productivity, an increasing $CaCO_3$ weathering flux, and an increasing deep-sea $CaCO_3$ burial flux. The majority of our simulations also predict an increase in terrestrial carbon, coupled with a decrease in ocean and increase in lithospheric carbon. An initial comparison of these dominant changes with observations and paleo-proxies suggests broad agreement. However, a comparison against carbon isotope data would be needed for a more robust assessment.

1 Introduction

Analyses of Antarctic ice core records suggest that the atmospheric CO_2 concentration at the Last Glacial Maximum (LGM), about 21 kyr ago, was around 190 ppmv, well below the preindustrial atmospheric concentration of around 280 ppmv. The most commonly accepted mechanisms to explain the atmospheric CO_2 decrease include lower sea surface temperatures (Martin et al., 2005; Menviel et al., 2012), iron fertilisation (Bopp et al., 2003; Oka et al., 2011; Jaccard et al., 2013; Ziegler et al., 2013; Martínez-Garcia et al., 2014; Lambert et al., 2015), sea-ice capping of air-sea gas exchange (Stephens and Keeling, 2000; Sun and Matsumoto, 2010; Chikamoto et al., 2012) and ocean circulation/stratification changes (Adkins et al., 2002; Lynch-Stieglitz et al., 2007; Skinner et al., 2010; Lippold et al., 2012; Gebbie, 2014; Skinner et al., 2014; Tiedemann et al., 2015; de la Fuente et al., 2015; Freeman et al., 2015), due to a range of possible mechanisms such as increased brine rejection (Shin et al., 2003; Bouttes et al., 2010, 2011; Zhang et al., 2013; Ballarotta et al., 2014), a shift in/weakening of the westerly wind belt over the Southern Ocean (Toggweiler et al., 2006; Anderson et al., 2009; Völker and Köhler, 2013), stronger westerly winds over the North Atlantic (Muglia and Schmittner, 2015), and a reduced or reversed buoyancy flux from the atmosphere to the ocean surface in the Southern Ocean (Watson and Garabato, 2006; Ferrari et al., 2014). A process that is conversely assumed to have contributed to increasing atmospheric $\mathrm{CO_2}$ is increasing salinity and ocean total dissolved inorganic carbon (DIC) concentration in response to decreasing sea level (Ciais et al., 2013).

A dominant assumption is also that the terrestrial biosphere carbon inventory was reduced (Crowley et al., 1995; Adams and Faure, 1998; Ciais et al., 2012; Peterson et al., 2014), in line with independent estimates of an ocean carbon inventory that was enhanced by several hundred petagrams (Goodwin and Lauderdale, 2013; Sarnthein et al., 2013; Allen et al., 2015; Skinner et al., 2015; Schmittner and Somes, 2016). The decrease in terrestrial carbon is generally attributed to unfavourable climatic conditions for photosynthesis, and the destruction of organic material by moving ice sheets (e.g. Otto et al., 2002; Prentice et al., 2011; Brovkin et al., 2012; O'ishi and Abe-Ouchi, 2013). The hypothesis that there was an increase in terrestrial carbon has, however, also been put forward (e.g. Zeng, 2003; Zimov, 2006), with some studies additionally suggesting little net change (e.g. Brovkin and Ganopolski, 2015). Processes proposed to be responsible for the terrestrial carbon increase include growth in 'inert' or permafrost carbon, slower 'active' soil respiration rates, continental shelf regrowth, and the preservation rather than destruction of terrestrial biosphere carbon in areas to be covered by the expanding Laurentide and Eurasian ice sheets (Weitemeyer and Buffett, 2006; Franzén and Cropp, 2007; Zeng et al., 2007; Zimov et al., 2009; Zech et al., 2011).

Other mechanisms which may have affected the LGM atmospheric $\mathrm{CO_2}$ change include changes in carbonate weathering rate, through its control on the ocean ALK:DIC ratio and consequently the solubility of $\mathrm{CO_2}$ (Munhoven, 2002; Jones et al., 2002; Foster and Vance, 2006; Vance et al., 2009; Brovkin et al., 2012; Crocket et al., 2012; Lupker et al., 2013; Simmons et al., 2016), decreasing dissolved organic carbon inventory due to a more stratified deep ocean (Ma and Tian, 2014), reduced shallow water carbonate deposition, which has the opposite impact of increased carbonate weathering rates (Opdyke and Walker, 1992; Kleypas et al., 1997; Brovkin et al., 2007), reduced marine bacterial metabolic rate in response to lower ocean temperatures, which acts to decrease the return rate of DIC from the remineralisation of organic material (Matsumoto et al., 2007; Roth et al., 2014), silicic acid leakage, or the leaking out of silicic acid trapped in the Southern Ocean to fuel diatom production, and hence potentially enhancing the uptake of $\mathrm{CO_2}$ (Matsumoto et al., 2002, 2014), Si fertilisation or the fertilization of diatom productivity in response to increased Si inventory (Harrison, 2000; Tréguer and Pondaven, 2000) and increased oceanic PO_4 inventory, due to e.g. lower sea level, alleviating the PO_4 limitation on marine production (Tamburini and Follmi, 2009; Wallmann, 2014, 2015).

Mechanisms put forward to explain the LGM atmospheric CO_2 decrease arise from paleo-data and model studies. The latter most often involve factorial experiments, introducing mechanisms one at a time. There is rarely any investigation of the impact of alternative assumptions regarding parameter values or model structure. Here, our aim is conversely to take an uncertainty-based approach to investigating the LGM CO_2 drop by simulating it with a large ensemble of parameter sets designed to allow for a wide range of large-scale feedback response strengths (Holden et al., 2013a). The objective is not to definitely explain the causes of the CO_2 drop but rather explore the range of possible responses. By *responses* we mean physical and biogeochemical changes in the Earth System (e.g. change in global particulate organic carbon export flux) and how these might be linked to ΔCO_2 and to each other, rather than specific mechanisms (e.g. iron fertilisation). In this study, we furthermore seek to simulate the LGM atmospheric CO_2 drop with the simulated CO_2 feeding back to the simulated climate, which is still infrequently done in LGM CO_2 experiments, and the first time it is done with GENIE-1. Moreover, rather than assuming that terrestrial carbon gets destroyed by the LGM ice sheets, we assume that it gets gradually buried. This assumption has not yet been implemented in an equilibrium set-up.

Despite our ensemble varying many of the parameters thought to contribute to variability in glacial-interglacial atmospheric CO_2, not all sources of uncertainty can be captured, and this is reflected in our simulated ΔCO_2 distribution. We estimate that up to ~60 ppmv of ΔCO_2 could be due to processes not included in our model and error in our process representations (see section 2.4 for details). We thus treat simulations with ΔCO_2 between ~-90 and -30 ppmv as “equally plausible”, and focus on describing the physical and biogeochemical changes seen in this subset. We also do an initial assessment of how the subset mean and/or dominant (in terms of sign) responses compare against observations and paleo-proxies, including temperature, sea ice, precipitation, AMOC & AABW cell strengths, terrestrial carbon, ocean carbon, particulate organic matter export and deep-sea $CaCO_3$ burial.

Finally, to test the robustness of relationships derived from the analysis of the ensemble subset with ΔCO_2 between ~-90 and -30 ppmv, we briefly compare the physical and biogeochemical changes seen therein with the changes seen in the ensemble with no ΔCO_2 filter, and the ensemble with a more negative ΔCO_2 filter (~-90 to -60 ppmv) (section 2.4). In general, the same dominant relationships between ΔCO_2 and the physical and biogeochemical changes are observed as in the subset with ΔCO_2 between ~-90 and -30 ppmv. In the case of the ensemble subset with ΔCO_2 between -90 and -60 ppmv, we additionally look at what proportion of the total terrestrial carbon change comes from within the ice sheet areas, and from there draw conclusions for the rest of the ensemble.

The paper is organised as follows. The introduction section, Section 1, is followed by Section 2, which describes the model, the ensemble, the simulation set-up and the ensemble subsets to be analysed. Section 3 is the results and discussion section, which includes a brief evaluation of the preindustrial (control) spin-up simulation to verify reproducibility of Holden et al., 2013a. The majority of the section is devoted to the LGM simulation: namely, diagnosis of the physical and biogeochemical changes (including potential causal relationships) seen in the subset with ΔCO_2 between ~-30 and -90 ppmv, and to a lesser extent, the ensemble with both more and less constrained ΔCO_2. Comparison of the first subset against observations and paleo-proxies is also included. Section 4 provides the key conclusions.

2 Methods

2.1 The model

The GENIE-1 configuration is as described in Holden et al. (2013a). The physical model consists of a three-dimensional frictional geostrophic ocean model (GOLDSTEIN) coupled to a thermodynamic/dynamic sea ice model (Edwards and Marsh, 2005; Marsh et al., 2011) and a two-dimensional Energy-Moisture Balance Model (EMBM). Atmospheric tracers are a sub-component of the EMBM, with a simple module (ATCHEM) used to store the concentration of atmospheric gases and their relevant isotopic properties (Lenton et al., 2007). The model land surface physics and terrestrial carbon cycle are represented by ENTS (Williamson et al., 2006). The ocean biogeochemistry model (BIOGEM) is as described in Ridgwell et al. (2007) but includes a representation of iron cycling (Annan and Hargreaves, 2010), and the biological uptake scheme of Doney et al. (2006). The model sediments are represented by SEDGEM (Ridgwell and Hargreaves, 2007). GENIE-1 also includes a land surface weathering model, ROKGEM (Colbourn, 2011), which redistributes prescribed weathering fluxes according to a fixed river-routing scheme. The model is on a 36 x 36 equal-area horizontal grid, with 16 vertical levels in the ocean.

2.2 The ensemble

The GENIE-1 ensemble consists of 471 parameter sets, varying 29 key model parameters over the ranges in Table 1. It derives from the 471-member EFPC ensemble of Holden et al. (2013a), which varies 24 active parameters and 1 dummy parameter (as a check against over-fitting). The parameter values in Holden et al. (2013a) were derived by building emulators of eight preindustrial climate metrics and applying a rejection sampling method known as approximate bayesian computation (ABC) to find parameter sets that the emulators predicted were modern plausible. Two parameters were later added to the EFPC ensemble in Holden et al. (2013b) to describe the un-modelled response of clouds to global average temperature change (OL1), and the uncertain response of photosynthesis to changing atmospheric CO_2 concentration (VPC).

We add two further parameters here that represent uncertain processes specific to the LGM. The first (FFX) scales ice-sheet meltwater fluxes to account for uncertainty in un-modelled isostatic depression at the ice-bedrock interface due to ice sheet growth, and for assuming a fixed land-sea mask (Holden et al., 2010b) We vary the parameter in the ensemble to capture the uncertainty in the magnitude of the glacial sea level drop and its effects on the carbon cycle.The second (GWS) scales the global average carbonate preindustrial weathering rates for the LGM, to account for uncertainty in carbonate weathering and un-modelled shallow water carbonate deposition rate changes. For both FFX and GWS, uniform random values were derived using the generation function runif in R.

Table 1. Ensemble parameters. Ranges are from (a) Holden et al. (2013a), (b) Holden et al. (2013b), and (c) Holden et al. (2010b), with the exception of GWS (see main text). The table also precludes the dummy parameter.

Module	Code	Description	Range	Ref.
EMBM	AHD	Atmospheric heat diffusivity ($m^2\ s^{-1}$)	1118875 to 4368143	a
	AMD	Atmospheric moisture diffusivity ($m^2\ s^{-1}$)	50719 to 2852835	a
	APM	Atlantic-Pacific moisture flux scaling	0.1 to 2.0	a
	OL0	Clear skies OLR reduction ($W\ m^{-2}$)	2.6 to 10.0	a
	OL1	OLR feedback ($W\ m^{-2}\ K^{-1}$)	-0.5 to 0.5	b
GOLDSTEIN	OHD	Isopycnal diffusivity ($m^2\ s^{-1}$)	312 to 5644	a
	OVD	Reference diapycnal diffusivity ($m^2\ s^{-1}$)	0.00002 to 0.0002	a
	OP1	Power law for diapycnal diffusivity depth profile	0.008 to 1.5	a
	ODC	Ocean inverse drag coefficient (days)	0.5 to 5.0	a
	WSF	Wind scale factor	1.0 to 3.0	a
	FFX	Freshwater flux scaling factor	1.0 to 2.0	c
SEA-ICE	SID	Sea ice diffusivity ($m^2\ s^{-1}$)	5671 to 99032	a
ENTS	VFC	Fractional vegetation dependence on vegetation carbon density ($m^2\ kgC^{-1}$)	0.4 to 1.0	a
	VBP	Base rate of photosynthesis ($kgC\ m^{-2}\ yr^{-1}$)	3.0 to 5.5	a
	VRA	Vegetation respiration activation energy ($J\ mol^{-1}$)	24211 to 71926	a
	LLR	Leaf litter rate (yr^{-1})	0.08 to 0.3	a
	SRT	Soil respiration activation temperature (K)	198 to 241	a
	VPC	Photosynthesis half-saturation to CO_2 (ppmv)	30 to 697	b
BIOGEM	PHS	PO_4 half-saturation concentration ($mol\ kg^{-1}$)	5.3e-8 to 9.9e-7	a
	PRP	Initial proportion of POC export as recalcitrant fraction	0.01 to 0.1	a
	PRD	e-folding remineralisation depth of non-recalcitrant POC (m)	106 to 995	a
	RRS	Rain ratio scalar	0.02 to 0.1	a
	TCP	Thermodynamic calcification rate power	0.2 to 2.0	a
	PRC	Initial proportion of $CaCO_3$ export as recalcitrant fraction	0.1 to 1.0	a
	CRD	e-folding remineralisation depth of non-recalcitrant $CaCO_3$ (m)	314 to 2962	a
	FES	Iron solubility	0.001 to 0.01	a
	ASG	Air-sea gas exchange parameter	0.1 to 0.5	a
ROKGEM	GWS	Land-to-ocean bicarbonate flux scaling factor	0.5 to 1.5	n/a

2.3 Experimental set-up of the model

The preindustrial ensemble simulation results were repeated to verify reproducibility of Holden et al. (2013a). The simulations were performed in two stages, each lasting 10 kyr, on the Cambridge High Performance Computing (HPC) Cluster Darwin. The first stage involved spinning up the model with atmospheric CO_2 concentration relaxed to 278 ppmv and a closed biogeochemistry system. This means that there are no sediment-ocean interactions and the model forces the $CaCO_3$ weathering and deep sea sediment burial rates into balance. An initial $CaCO_3$ weathering is initially prescribed but this is subsequently rescaled internally to balance the modelled $CaCO_3$ burial rate and conserve alkalinity. In the second stage, atmospheric CO_2 was allowed to evolve freely, with interacting oceans and sediments, and the $CaCO_3$ weathering rate is set equal to the $CaCO_3$ burial rate diagnosed from the end of stage 1.. To allow the sediments to reach equilibrium as fast as possible, no bioturbation was modelled in either stage 1 or stage 2.

Each parameter set was then applied to LGM simulations. The modelled preindustrial equilibrium states were used as initial conditions and the ensemble members were integrated for 10 kyr, with freely evolving CO_2. These 10 kyr simulations are variously referred to here as the “LGM equilibrium simulation” or “stage 3”, and the LGM equilibrium state refers to the end of stage 3 (see S1 for more details).. After application to stages 2 and 3, the original 471 ensemble members were filtered to 315 ensemble members to exclude those simulations with a stage 2 atmospheric CO_2 concentration outside of the range 268 to 288 ppmv (c.f. Prentice et al., 2001), which entered a snowball Earth state in stage 3 or which showed evidence of numerical instability (c.f. Holden et al., 2013b).

Boundary conditions applied in the LGM simulations included orbital parameters (Berger, 1978) and aeolian dust deposition fields (Mahowald et al., 2006). The atmospheric CO_2 used in the radiative code is internally generated, rather than prescribed but the radiative forcing from dust, and gases other than CO_2 was neglected. The model also requires a detrital flux field to the sediments, containing contributions from opal and material from non-aeolian sources (Ridgwell and Hargreaves, 2007). Weathering fluxes from the preindustrial simulation were applied, scaled by GWS.

The representation of the ice sheets is as described in Holden et al. (2010b), using the terrestrial ice sheet fraction and orography from the ICE-4G reconstruction of Peltier (1994). Rather than initialising the ensemble with the ice sheet extent and orography at 21 kyr BP, the ice sheets are configured to grow from their preindustrial to LGM extent in 1 kyr, at the beginning of the LGM simulation (i.e. years 0-1 kyr) in order to account for the impact of sea level change on ocean tracers. Following Holden et al. (2010b), only the Laurentide and Eurasian Ice Sheets are allowed to change from their preindustrial form (accounting for

~ 80% of global ice sheet change), and we also route the freshwater to build the ice sheets from the Atlantic, Pacific and Arctic, assuming modern topography, rather than extracting it uniformly.

As discussed in the introduction, the preindustrial terrestrial carbon is preserved underneath the LGM ice sheets, and allowed to interact with the atmosphere prior to its burial. To determine how sensitive the burial carbon amount is to the duration of ice sheet build-up, we test the impact of varying the latter from 1000 to 10,000 years for one ensemble member (extending the total simulation length to 11,000 years). Our assumption is that if the difference is negligle, applying the same ensemble member to a transient simulation of the full glacial cycle (and therefore a more realistic ice sheet build-up history) would not have yielded a dramatically different burial carbon inventory. We find that increasing the ice sheet build-up duration indeed changes the burial carbon amount only marginally (~34 PgC). A limitation, however, is that we do not have a way of testing if other ensemble members may be more sensitive. If one expects the sign of their response to be the same, more sensitive here means more carbon, not less, buried underneath the ice sheet.

2.4 Ensemble subsets

Although our ensemble varies many of the parameters thought to contribute to variability in glacial-interglacial atmospheric CO_2, not all sources of uncertainty can be captured. We estimate that up to ~60 ppmv of ΔCO_2 could be due to error in our process representations and processes not included in our model, such as changing marine bacterial metabolic rate, wind speed (via its effect on gas transfer) and Si fertilization. This is not a comprehensive assessment, however, as our model also does not include processes such as the effect of changing winds on ocean circulation (Toggweiler et al., 2006), Si leakage (Matsumoto et al., 2002, 2013, 2014), the effect of decreasing SSTs on $CaCO_3$ production (Iglesias-Rodriguez et al., 2002), or changing oceanic PO_4 inventory (Menviel et al., 2012). We focus our analyses on the subset of the ensemble with ΔCO_2 between ~-90 and -30 ppmv (Table 2), treating each ensemble member in this range as equally plausible. To test the robustness of diagnosed relationships, we also briefly compare the reponse of this subset with the response of the ensemble with no ΔCO_2 filter, and the response of the ensemble with a more negative ΔCO_2 filter. In the latter case, the upper ΔCO_2 limit is set to ~-60 ppmv, roughly equivalent to allowing for an extra atmospheric CO_2 decrease due to changing marine bacterial metabolic rate, wind speed (via its effect on gas transfer) and Si fertilization, between the best and upper estimate of Kohfeld and Ridgwell (2009). The ΔCO_2 distribution in each subset or ensemble is shown in Fig. 1.

Table 2. Ensemble subsets, including ΔCO_2 and number of members in each.

Ensemble	ΔCO_2 range (ppmv)	Number of members
ENS_{315}	-88 to 74	315
ENS_{104}	-88 to -30	104
ENS_{16}	-88 to -59	16

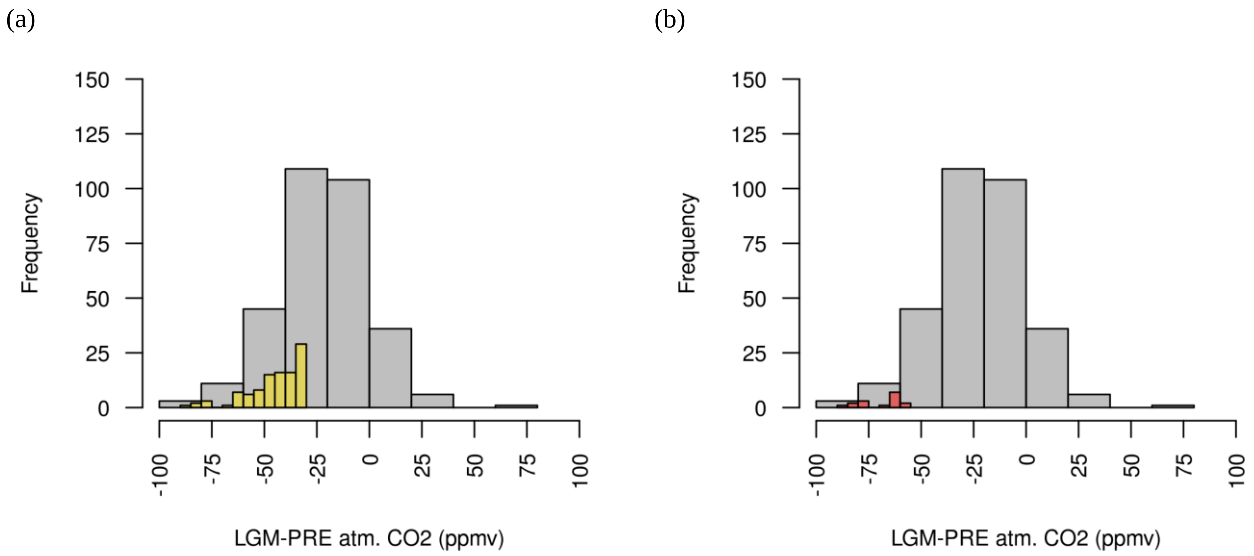

Fig. 1. LGM change in atmospheric CO_2 (a-b) distribution. The ENS_{315} response is shown in grey, the ENS_{104} ensemble response in yellow and the ENS_{16} ensemble response in purple. Unless otherwise specified, the same colour legend applies to all figures in the manuscript.

3 Results and discussion

3.1 Preindustrial simulations

Comparison of the preindustrial response of ENS_{315} (i.e. the original, non-$\Delta\mathrm{CO}_2$ filtered ensemble) against the preindustrial ensemble response of Holden et al., 2013a confirms that the two are very similar. We additionally evaluate ENS_{315} against a few additional preindustrial metrics (see S2) and find responses that can be deemed not uncontroversially implausible, following the design principles for the ensemble, outlined in Holden et al., 2013a.

3.2 LGM simulations

3.2.1 Climate, sea level and ocean circulation

Temperature

The ENS_{104} mean LGM surface air temperature (SAT) anomaly ($\Delta\mathrm{SAT}$) is -4.6 $\pm$ 1.7, and the range is -2.5 to -10.4 °C. The mean is close to the observed $\Delta\mathrm{SAT}$ of -4 $\pm$ 1 °C (Annan and Hargreaves, 2013), and the range roughly equivalent to the range of previous model-based estimates (Kim et al., 2003; Masson-Delmotte et al., 2006; Schneider von Deimling et al., 2006; Braconnot et al., 2007; Holden et al., 2010a; Brady et al., 2013). The ENS_{104} mean LGM SST anomaly (ΔSST) is -1.8 ± 0.8 °C, and the range is -4.5 and -0.7 °C. The mean is again close to an observational data-constrained model estimate (Schmittner et al. (2011), and within the range of estimates inferred from proxy data (MARGO Project Members 2009 in Masson-Delmotte et al., 2013). There is a positive correlation between $\Delta\mathrm{SAT}$ and $\Delta\mathrm{CO}_2$ (r = 0.75, 0.05 significance level hereforth), most likely reflecting the radiative impact of atmospheric CO_2 on SAT, as well as the effect of changing SAT on $\Delta\mathrm{CO}_2$. As suggested above, decreasing SST may contribute to decreasing CO_2 via the CO_2 solubility temperature dependence. Changing SAT may also affect $\Delta\mathrm{CO}_2$ via its effects on sea ice, ocean circulation, terrestrial and marine productivity (see below). The positive correlation is reproduced in ENS_{315} (r = 0.74), and $\Delta\mathrm{SAT}$ and $\Delta\mathrm{SST}$ tend to be less negative in ENS_{315} than in ENS_{104} (Fig. 2). In ENS_{16}, $\Delta\mathrm{SAT}$ and $\Delta\mathrm{SST}$ are from the extreme or at least lower end of the ENS_{104} range.

The ENS_{104} mean $\Delta\mathrm{SAT}$ and $\Delta\mathrm{SST}$ spatial distributions are shown in Fig. 3. In line with observations (Annan and Hargreaves, 2013), the largest SAT decreases (> 10 °C) are simulated over the Laurentide and Eurasian Ice Sheets. The equator to pole temperature gradient is also broadly reproduced. The largest SST decreases (≥ 4 °C) are found in the North Atlantic and northeast Pacific, with more limited cooling (≤ -2 °C) in the tropics and polar regions, again consistent with observations. The largest SST decreases ought to, however, also be found in the southern hemisphere mid-latitudes whereas the simulate cooling is more moderate.

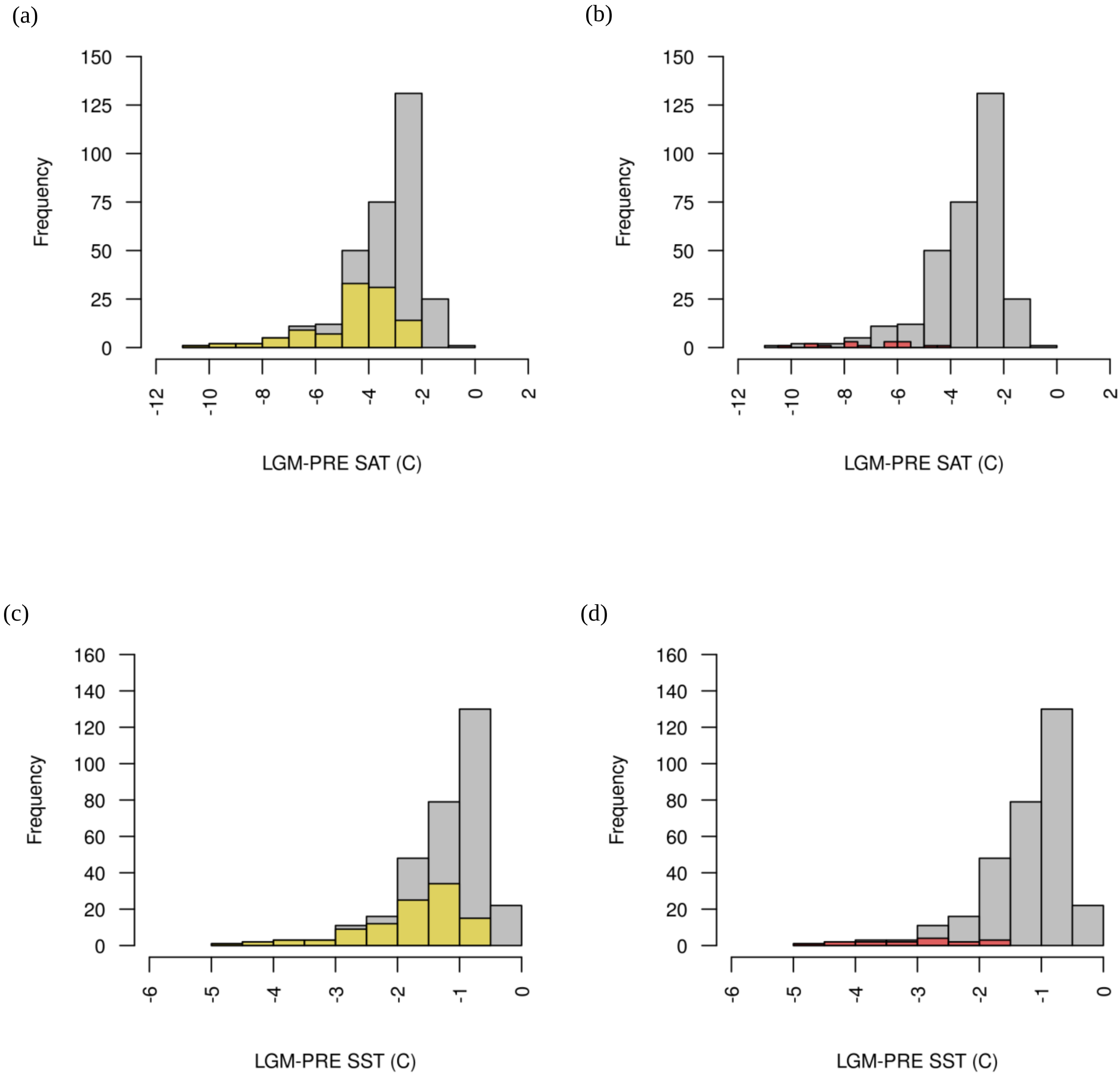

Fig. 2. LGM change in surface air temperature (a-b) and sea surface temperature (c-d) distributions.

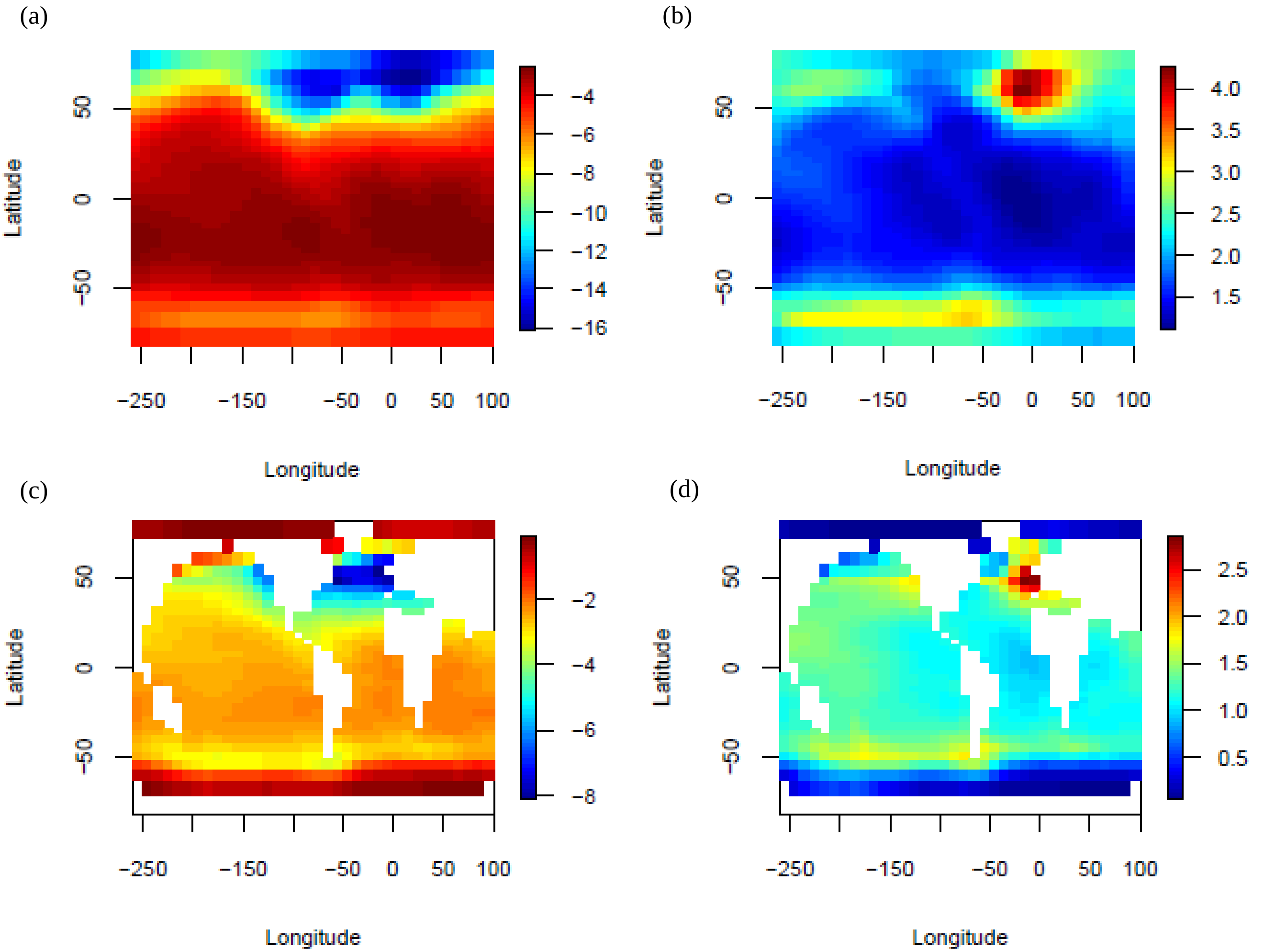

Fig. 3. LGM change in surface air temperature (a-b) and sea surface temperature (c-d) (°C) ENS$_{104}$mean (left) and standard deviation (right).

Sea level

The ENS$_{104}$ mean percentage increase in LGM salinity (%S) (and DIC, ALK, PO$_4$, etc) due to decreasing sea level is 2.84 $\pm$ 0.62 and the range is 2 to 4. There is no significant relationship between %S and ΔCO_2, and the distribution of %S is similar in ENS$_{104}$ than in both ENS$_{315}$ and ENS$_{16}$ (Fig. 4). There is, however, a weak positive correlation between %S and ΔCO_2 in ENS$_{315}$ (r = 0.17).

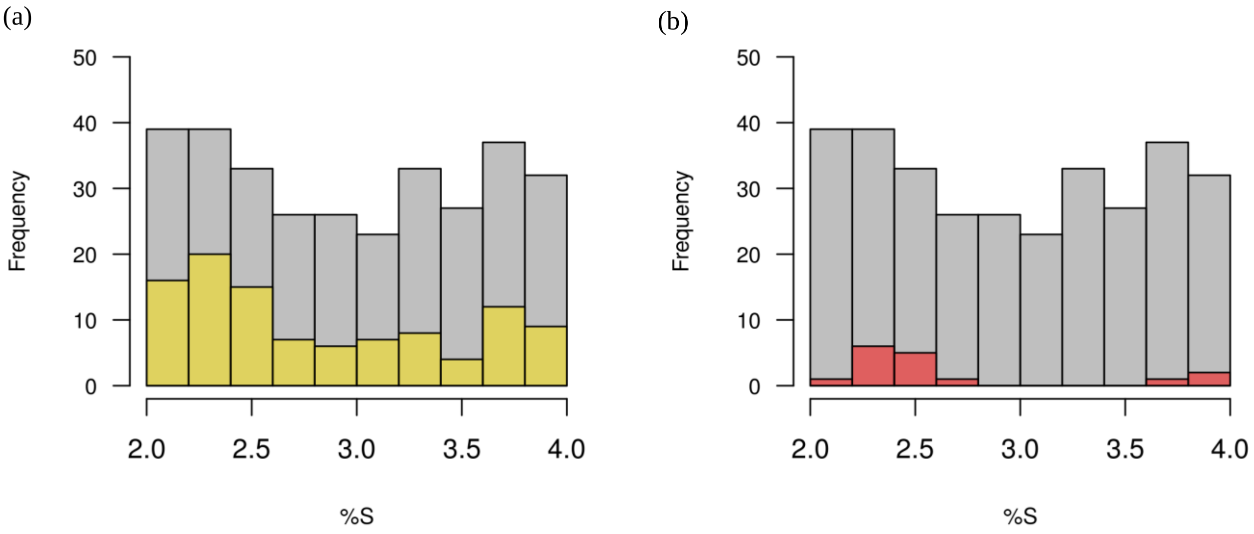

Fig. 4. Percentage increase in LGM salinity due to decreasing seal level (a-b) distribution.

Sea ice

The ENS$_{104}$ mean LGM global annual sea ice area anomaly (ΔSIA) is 18.6 $\pm$ 7.4 million km^2, and the range is 9.9 to 44 million km^2. There is a negative correlation between ΔSIA and ΔSAT (r = -0.97) and between ΔSIA and ΔCO_2 (r = -0.74).. The negative correlation between ΔSIA and ΔCO_2 likely reflects the impact of changing atmospheric CO_2 on ΔSIA but may also include a smaller contribution from changing sea ice area to ΔCO_2. Increasing LGM sea ice area may have for instance reduced the outgassing of CO_2 from the ocean, particularly in the Southern Ocean via sea ice capping, and reduced the net ocean-atmosphere CO_2 flux by decreasing the AMOC strength (see below). The negative correlation between ΔSIA and ΔSAT, and between ΔSIA and ΔCO_2, is reproduced in ENS$_{315}$ (r = -0.96 and r = -0.74 respectively). ΔSIA in ENS$_{104}$ also tends to be higher than in ENS$_{315}$, and smaller than in ENS$_{16}$ (Fig. 5).

As shown in Fig. 6, fractional sea ice cover increases in all regions where sea ice is present in preindustrial simulations, although the largest increases take place in the North Atlantic.

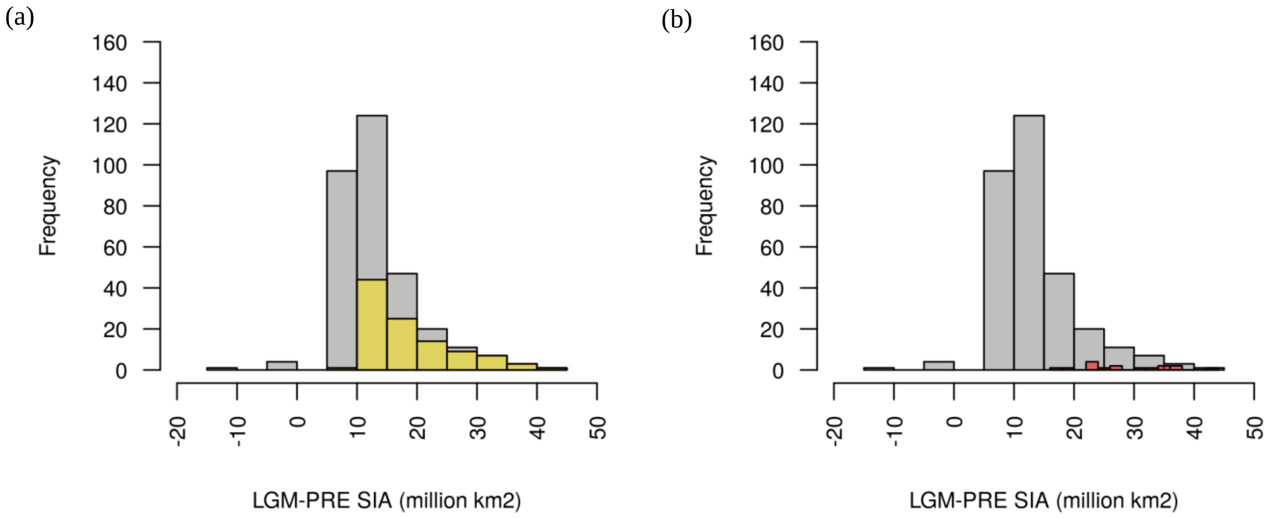

Fig. 5. LGM change in global sea ice area (a-b) distribution.

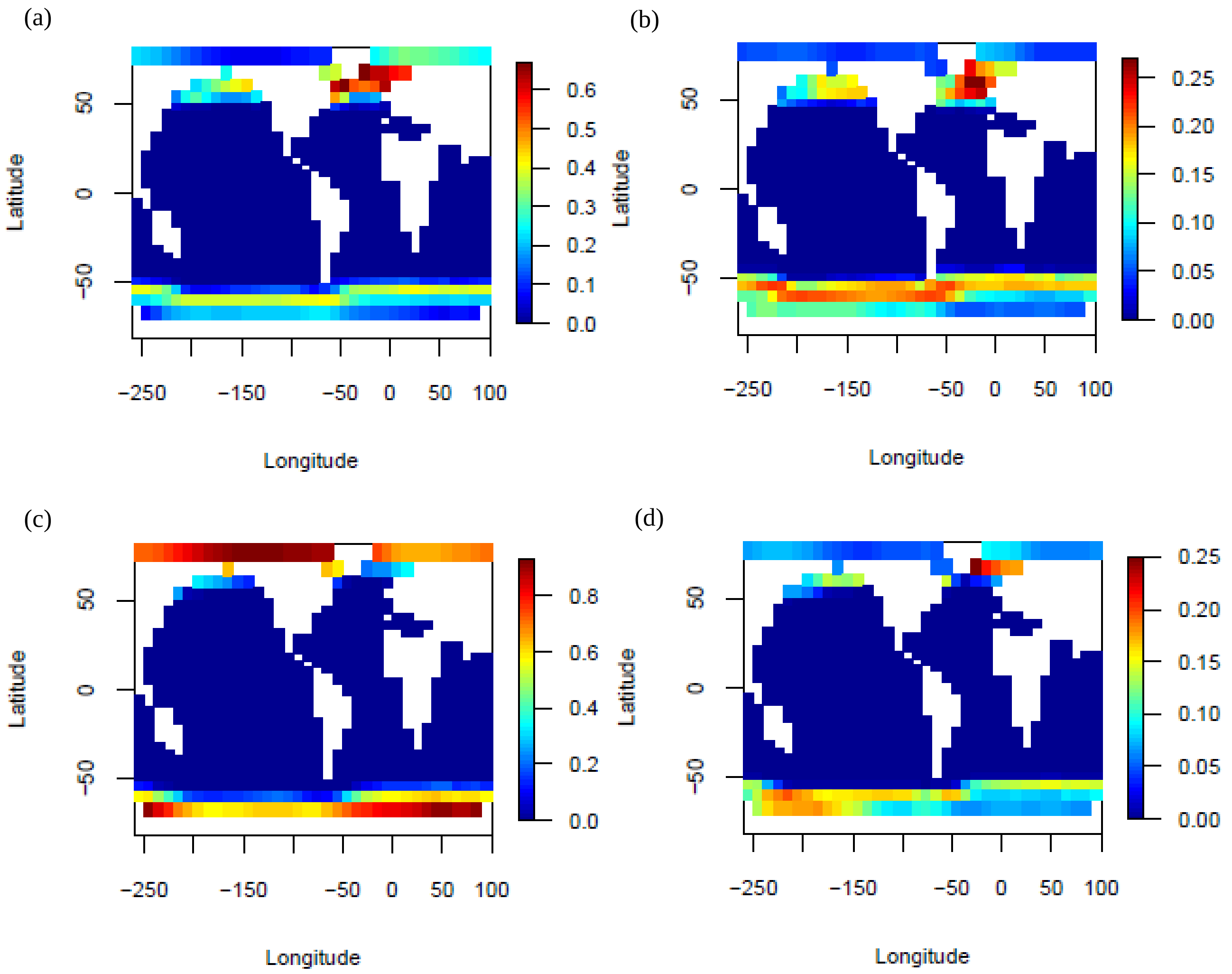

Fig. 6. LGM-PRE (a-b) and PRE (c-d) fractional sea ice cover ENS$_{104}$means (left) and standard deviations (right).

Precipitation

The ENS_{104} mean spatial distribution of the LGM precipitation rate anomaly (ΔPP) is shown in Fig. 7. The LGM changes are mostly negative but regions of positive ΔPP do exist, notably over Siberia and Australia. The largest LGM precipitation decreases (> 1.5 mm day $^{-1}$, with a maximum of 2.25 mm day $^{-1}$) are found over northern North America, and from around the eastern North Atlantic to northwest Asia, coinciding with the location of the Laurentide and Eurasian Ice Sheets (and the largest increases in fractional sea ice cover) respectively. Relatively large precipitation decreases (> 0.75 mm day $^{-1}$) are also simulated across China, equatorial Africa and other regions of enhanced fractional sea ice cover. Comparison against a pollen-based precipitation reconstruction (Bartlein et al., 2011 in Alder and Hostetler, 2015) suggest that the simulated precipitation changes over Europe and equatorial Africa are of the right direction, while precipitation changes over western Siberia at least ought to be negative. The sign of the precipitation changes over North America is mostly consistent with observations, which record negative changes over most of the continent. However, positive changes, which are also observed, are not captured. Although not shown here, comparison of the ENS_{104} mean against the ENS_{315}mean suggests that the precipitation patterns in the two are very similar, but the decreases generally tend to be higher in the ENS_{104}mean. The precipitation decreases in the latter conversely tend to be smaller than in ENS_{16}.

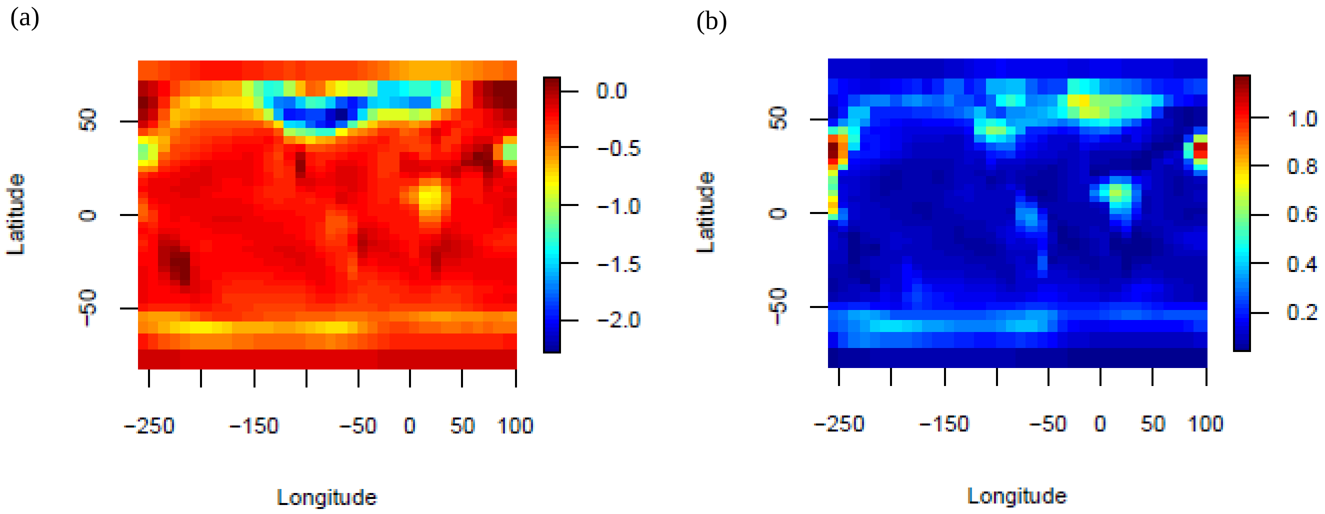

Fig. 7. LGM change in precipitation rate (mm day^{-1}) ENS_{104} mean (a) and standard deviation (b).

Ocean circulation

The ENS_{104} mean LGM AMOC strength anomaly ($\Delta\psi_{\max}$) is -2.8 ± 2.8 Sv, and the range is -8 to 4.7 Sv (Fig. 8). These estimates are at the low end of the $\Delta\psi_{\max}$ predicted by 9 PMIP2 (Weber et al., 2007) and 8 PMIP3 (Muglia and Schmittner, 2015) coupled model simulations. However, they do not include the more negative $\Delta\psi_{\max}$ predicted by Völker and Köhler (2013) for instance. The ENS_{104} mean LGM-PRE AABW cell strength in the Atlantic Ocean ($\Delta\psi_{\min}$) is 0.1 ± 1.2 Sv, which here represents an LGM decrease in cell strength as we keep the original (negative) sign for anticlockwise flow of Antarctic water. A negative $\Delta\psi_{\min}$ conversely represents an LGM increase in cell strength. The range of $\Delta\psi_{\min}$ is -4.3 to 4.3 Sv, roughly comparable to the range of $\Delta\psi_{\min}$ predicted in Weber et al. (2007) (see also Muglia and Schmittner, 2015), but excluding the much larger $\psi_{\min}$ increase predicted by Kim et al. (2003) for example.. The northern limits of the ENS_{104} mean LGM AMOC and AABW cells are roughly at the same latitudes as in the preindustrial simulations (Fig. 9). The maximum depth reached by the ensemble mean AMOC base is also similar to preindustrial. Observations (Lynch-Stieglitz et al., 2007; Lippold et al., 2012; Gebbie, 2014; Böhm et al., 2015), conversely, suggest that the LGM AMOC shoaled to < 2 km, raising its base depth by 2500 and 600 m at the north and south end of the return flow respectively. The LGM AABW, in turn, is thought to have filled the deep Atlantic below 2 km, reaching as far north as 65 °N, which is ca. 25 degrees north of its modern northern limit (Oppo et al., 2015).

Although not show here, the ENS_{16}ensemble members tend to exhibit a shoaling of the AMOC and enhanced penetration of AABW. With regard to $\Delta\psi_{\max}$ and $\Delta\psi_{\min}$, these tend to be more negative (i.e. weaker AMOC and stronger AABW) than in ENS_{104}. The $\Delta\psi_{\max}$ and $\Delta\psi_{\min}$ in ENS_{315} tend to conversely be more positive. In ENS_{104}, we also find a positive relationship between $\Delta\psi_{\max}$ and $\Delta\mathrm{CO}_2$ (r = 0.57) and a negative relationship between $\Delta\psi_{\min}$ and $\Delta\mathrm{CO}_2$ (r = -0.42). The relationships are reproduced in ENS_{315} (r = 0.59 and r = -0.36 respectively). We additionally find, in both ENS_{104} and ENS_{315}, negative correlations between $\Delta\psi_{\max}$ and $\Delta\psi_{\min}$ (r = -0.62 and -0.63), $\Delta\psi_{\min}$ and ΔSAT (r = -0.4 and -0.4) and $\Delta\psi_{\max}$ and $\Delta\mathrm{SIA}$ (r = -0.62 and -0.66), as well as positive correlations between $\Delta\psi_{\max}$ and ΔSAT (r = 0.68 and 0.66), and $\Delta\psi_{\min}$ and $\Delta\mathrm{SIA}$ (r = 0.37 and 0.42). Based on these relationships, we hypothesise that increasing LGM AABW strength led to an expansion of the AABW cell, with the latter restricting the AMOC to lower depths, and reducing its overturning rate (e.g. Shin et al., 2003). The increase in AABW strength was likely driven by increases in sea ice enhancing brine rejection. Sea ice increases in the North Atlantic may have additionally weakened the AMOC cell by locally reducing deep convection.

The relationships between $\Delta\psi_{\max}$, $\Delta\psi_{\min}$ and $\Delta\mathrm{CO}_2$ are also consistent with increasing $\psi_{\min}$ (decreasing $\psi_{\max}$) contributing to decreasing atmospheric CO_2. The replacement of NADW by AABW in the North Atlantic would have for instance led to a dissolution of deep sea sediment CaCO_3 due to AABW having a lower bottom water CO_3^{2-}concentration than NADW (see e.g. Yu et al., 2014). The increased CaCO_3 dissolution flux in turn raises the whole ocean alkalinity, lowering the atmospheric CO_2. Enhanced AABW production would have also caused the deep ocean to become more stratified, allowing more DIC to accumulate at depth, and promoting further $CaCO_3$ dissolution. A decrease in NADW formation on its own may have moreover lowered atmospheric CO_2 by reducing the outgassing of CO_2 at the ocean surface and the burial rate of deep sea $CaCO_3$ through the concomitant increase in deep sea DIC accumulation.Further investigation is, however, required to confirm these causal relationships.

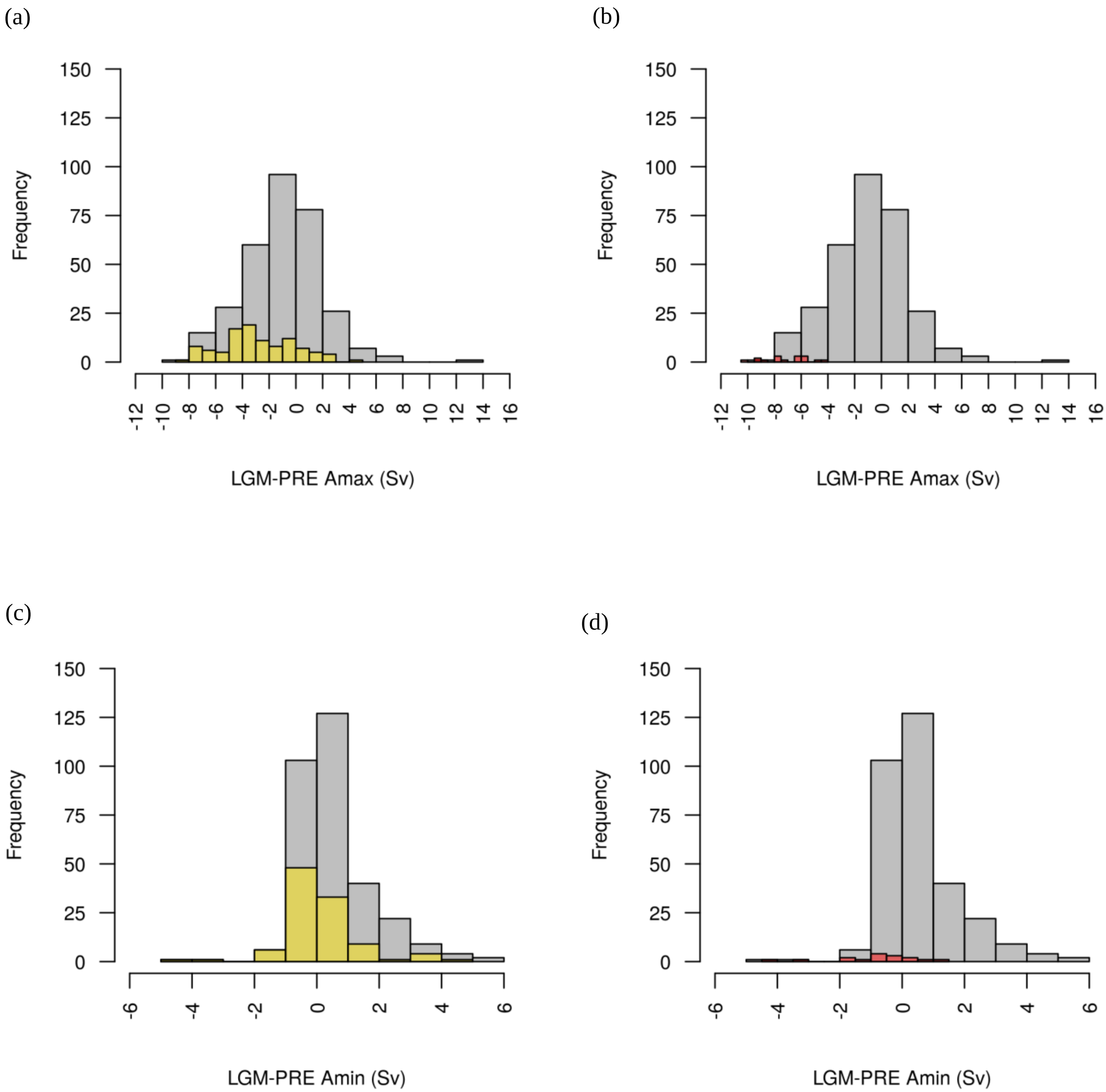

Fig. 8. LGM change in ψ_{max} (a-b) and ψ_{min} (c-d) distributions.

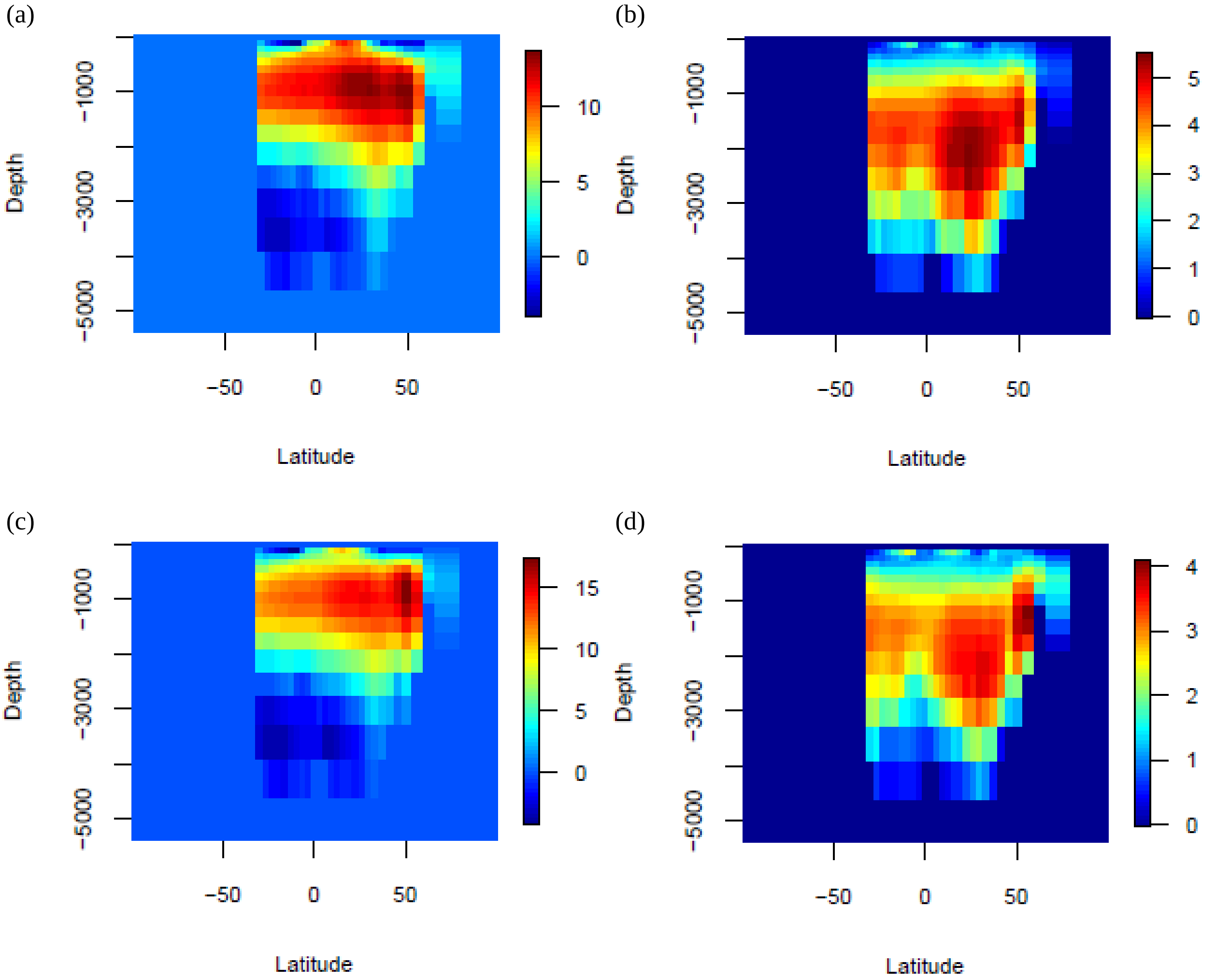

Fig. 9. LGM (a-b) and PRE (c-d) Atlantic overturning stream functions (Sv) ENS$_{104}$means (left) and standard deviations (right).

3.2.2 Terrestrial biosphere, ocean and lithospheric carbon

Most of the ensemble members in the PGACF ensemble predict an LGM increase in terrestrial biosphere ($\Delta\mathrm{TerrC}$), and lithospheric[1] ($\Delta\mathrm{LithC}$) carbon inventory and a decrease in ocean carbon inventory ($\Delta\mathrm{OceanC}$) (Fig. 10). The remaining ensemble members predict one of four other scenarios of carbon partitioning, with the second most common scenario (11% of ensemble members) being increasing terrestrial carbon and decreasing ocean and lithospheric carbon. Similar patterns can also be observed in ENS_{315} and ENS_{16} (Table 3). A likely explanation for scenario 1 is that the growth of biosphere carbon on land (see below) causes a flux of CO_2 from the atmosphere to the land, leading to immediate outgassing of CO_2 from the ocean to remove the atmospheric pCO_2 difference. The CO_2 outgassing also leads to an increase in surface $[\mathrm{CO}_3^{2-}]$ and subsequently deep ocean $[\mathrm{CO}_3^{2-}]$, which reduces CaCO_3 dissolution (and increases lithospheric carbon). The increase in CaCO_3 burial in turn decreases $[\mathrm{CO}_3^{2-}]$ and increases $[\mathrm{CO}_2]$, which is communicated back to the surface, with a resultant increase in atmospheric CO_2 (Kohfeld and Ridgwell, 2009). The above explanation is of course only part of the explanation for this dominant carbon partitioning scenario, with physical mechanisms also expected to play a role, in addition to any changes in ocean productivity and changes in land carbonate weathering (see below).

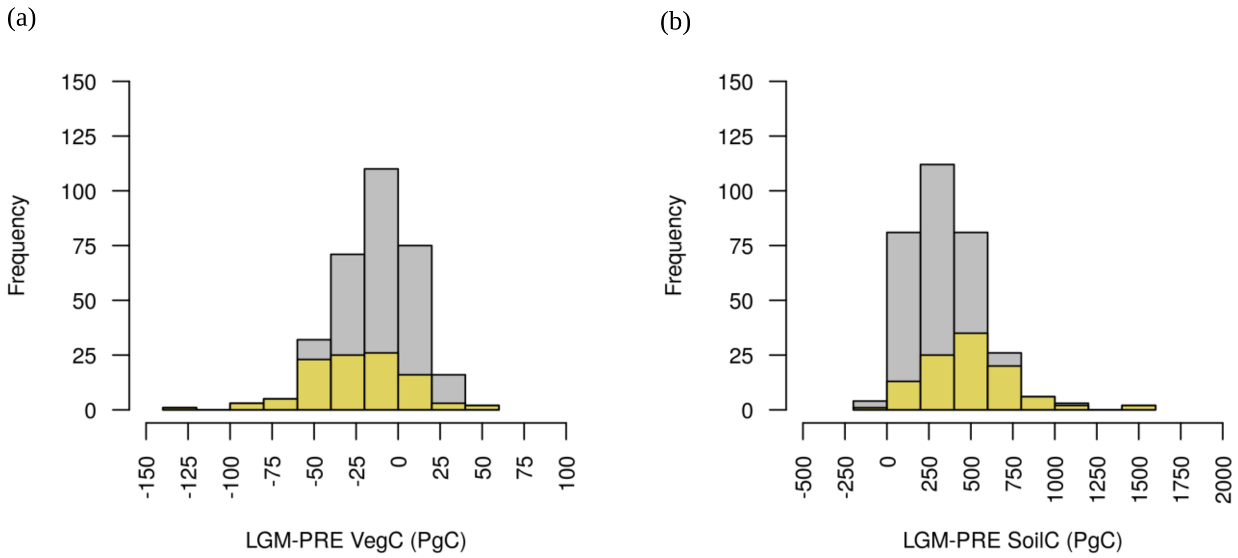

---

[1] The $\Delta\mathrm{LithC}$ stems from changes in the deep-sea CaCO_3 burial flux and/or CaCO_3 weathering/shallow water deposition flux and was initially calculated to ensure that carbon was being conserved over the LGM simulation.

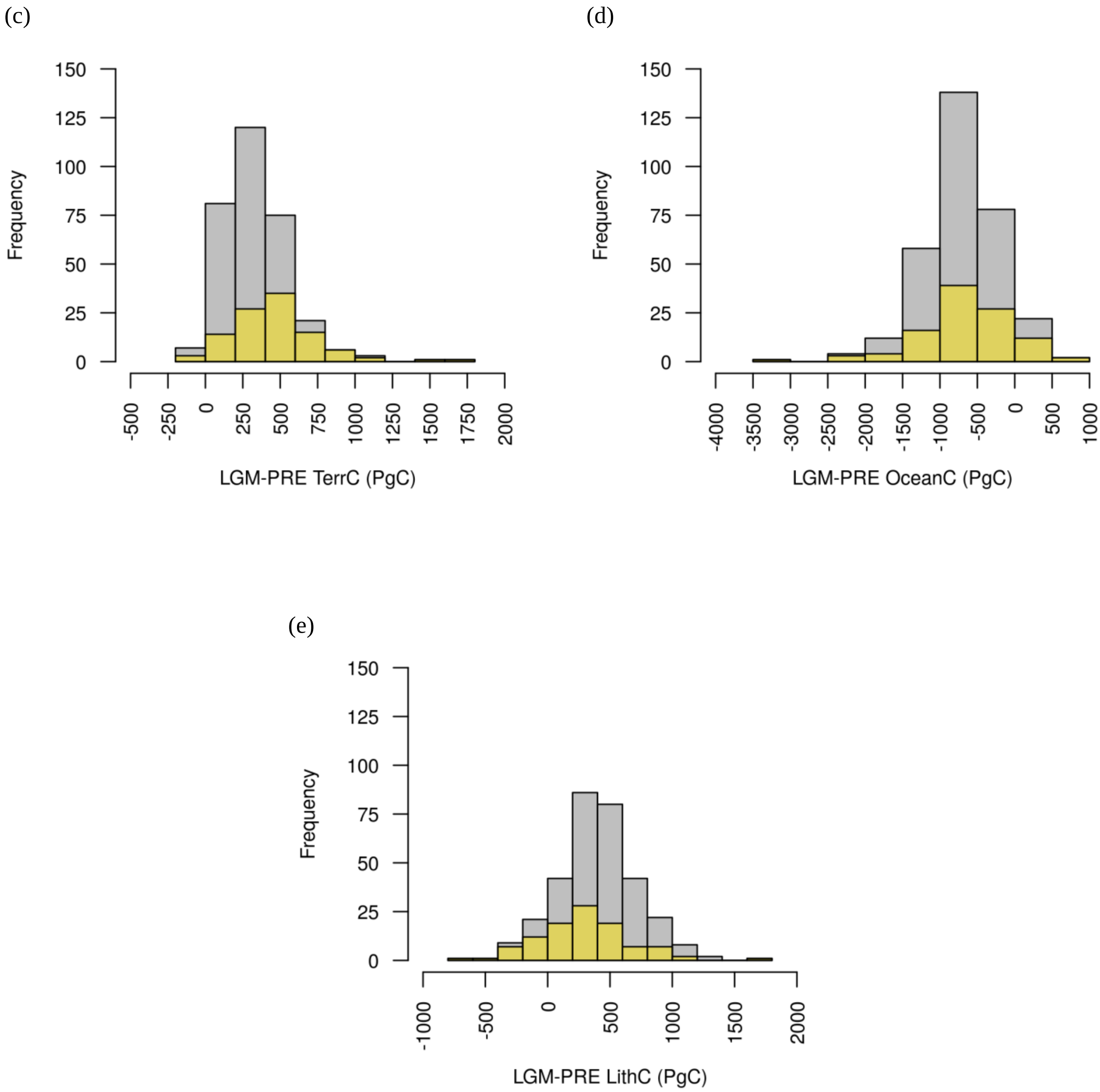

Fig. 10. LGM change in vegetation (a), soil (b), terrestrial (vegetation + soil) (c), ocean (d) and lithospheric (e) carbon inventory distributions.

Table 3. LGM-PRE carbon partitioning scenarios in ENS_{315}, ENS_{104} and ENS_{16}.

			ENS_{315}		ENS_{104}		ENS_{16}	
Scenarios			**Total counts**	**(% of total)**	Total counts	(% of total)	Total counts	(% of total)
1. ΔTerrC(+)	ΔOceanC(-)	ΔLithC(+)	279	(89)	82	(79)	10	(63)
2. ΔTerrC(+)	ΔOceanC(+)	ΔLithC(-)	16	(5)	11	(11)	3	(19)
3. ΔTerrC(+)	ΔOceanC(-)	ΔLithC(-)	11	(3)	8	(8)	2	(13)
4. ΔTerrC(-)	ΔOceanC(+)	ΔLithC(+)	1	(1)	1	(1)	0	(0)
5. ΔTerrC(-)	ΔOceanC(+)	ΔLithC(-)	5	(2)	2	(1)	1	(6)
6. ΔTerrC(-)	ΔOceanC(-)	ΔLithC(+)	1	(1)	0	(0)	0	(0)
7. ΔTerrC(+)	ΔOceanC(+)	ΔLithC(+)	2	(1)	0	(0)	0	(0)

The ENS_{104} mean ΔTerrC, ΔOceanC and ΔLithC, the signs of which are consistent with scenario 1, are reported in Table 4, alongside previous estimates from observational data- and model-based studies. From here we can see that the mean ΔTerrC is only aligned with a handful of estimates and no studies so far report a negative ΔOceanC. Instead, ΔOceanC is estimated to be positive, primarily based on carbon isotope data. The loss of hundreds of petagrams of carbon from the ocean in response to terrestrial carbon growth has, however, been previously proposed (e.g. Zimov et al., 2006). Moreover, if we assume that 90% of the atmospheric CO_2 perturbation caused by the increase in terrestrial biosphere carbon reported in Table 4 gets removed by the ocean and sediments, the change in ocean carbon would be negative, even after adding the remaining carbon to be lost from the atmosphere to the ocean. We discuss what these results would likely mean for carbon isotope data in section 3.2.6.

The positive ΔTerrC studies in Table 4 attribute the increase in terrestrial biosphere carbon to different factors: Zimov et al., 2009 and Zech et al., 2011 predict large increases in permafrost carbon while Zeng et al., 2003 ignores permafrost and instead attributes most of the glacial terrestrial carbon increase to ice sheet burial carbon. Another contributor is the storage of carbon on exposed continental shelves. Here, neither this carbon accumulation mechanism nor that of peat growth (absent also in Zeng, 2003), are included in our model. As discussed above, permafrost growth is also not represented explicitly but there is an attempt to capture the very slow rates of soil decomposition characteristic of permafrost (Williamson et al., 2006). Similarly to Zeng (2003), the model gradually buries carbon in LGM ice sheet areas. Analysis of ENS_{16} suggests that during the 1000 years of LGM ice sheet build-up, the terrestrial carbon inventory in the areas to be occupied by the ice sheets increases by between 6 and 444 PgC, yielding LGM ice-sheet carbon inventories (or "burial" carbon inventories) between 318 and 1341 PgC (Table 5). This increase accounts for less than half of the total LGM change in terrestrial carbon (i.e. $\Delta\mathrm{TerrC}$) in the majority of simulations. However, if this "extra" carbon (accumulated in response to climate forcings), and the carbon already present in the ice sheet areas at the end of the preindustrial spin-up, were to have been destroyed rather than preserved, ΔTerrC would be negative in all but 3 simulations, as opposed to positive in all but one simulation (Table 5).

Table 4. $\Delta\mathrm{TerrC}$, $\Delta\mathrm{OceanC}$ and $\Delta\mathrm{LithC}$ (PgC) in this study (ENS_{104} mean, standard deviation and range) and previous studies. PE14 = Peterson et al. (2014), OA13 = O'ishi and Abe-Ouchi (2013), C12 = Ciais et al. (2012), Z03 = Zeng (2003), SA13 = Sarnthein et al. (2013), BG15 = Brovkin and Ganopolski (2015), PR11= Prentice et al. (2011), SK15 = Skinner et al. (2015), SS16 = Schmittner and Somes (2016), GL13 = Goodwin and Lauderdale (2013), A15 = Allen et al. (2015), CR95 = Crowley et al. (1995), AF98 = Adams and Faure (1998), BR12 = Brovkin et al. (2012), ZI09 = Zimov et al. (2009), ZE11 = Zech et al. (2011).

	This study	Previous studies	Ref.	Details
$\Delta\mathrm{TerrC}$	467.5±286.5 [-51.6,1603.8]	[-1160, 530]	CR95	Pollen database
		-1500	AF98	Ecological data
		[-694, -550]	PR11	Simulation with LPX
		-600	BR12	Simulation with CLIMBER-2
		-597	OA13	Simulation with MIROC-LPJ
		-511	PE14	Benthic foraminiferal δ^{13}C records
		-330	C12	Benthic foraminiferal, ice core and terrestrial δ^{13}C records + simulation with LPJ land ecosystem model
		0	BG15	Simulation with CLIMBER-2 (+ permafrost, peat, glacial burial carbon)
		547	Z03	Simulation with a coupled atmosphere-land-ocean-carbon model
		[200, 400]	ZE11	Soil carbon measurements
		<1000	ZI09	Soil carbon measurements
$\Delta\mathrm{OceanC}$	-664±626.9 [-3187.7, 662.4]	[730, 980]	SA13	Ocean radiocarbon records
		687	SK15	Ocean radiocarbon records
		654	A15	Ocean $[\mathrm{CO}_3^{2-}]$ reconstructions + benthic foraminiferal δ^{13}C records
		[570, 970]	GL13	Ocean $[\mathrm{CO}_3^{2-}]$ reconstructions
		520	C12	Benthic foraminiferal, ice core and terrestrial δ^{13}C records + simulation with LPJ land ecosystem model
		[510,670]	SS16	Simulation with MOBI 1.5 coupled to Uvic
$\Delta\mathrm{LithC}$	292.5±373.9 [-654.9,1700.9]	n/a	n/a	n/a

Most of the increase in ice sheet carbon is due to soil carbon, with vegetation carbon decreasing in all but one simulation. The range of carbon inventory changes includes the 116 PgC increase in ice sheet carbon, and consequent total burial carbon inventory (431 PgC), estimated by Zeng (2003). It would also allow for an additional 250-550 PgC (Franzen, 1994) from increased glacial peat accumulation to be buried under the ice sheets, as suggested by Zeng (2003). No observational data-based estimates of the LGM burial carbon inventory are available since there is so far only limited evidence for organic material being preserved by ice during glaciations (Franzen, 1994 and references in Weitemeyer and Buffett, and Zeng, 2007). Outside of the ice sheets, increases in terrestrial carbon inventory are mostly due to soil carbon, which increases in all simulations. Vegetation carbon, conversely, decreases in the majority of simulations. The range of non-ice sheet carbon changes includes the 198 PgC increase in non-burial non-shelf terrestrial carbon predicted by Zeng (2003) as a result of reduced soil respiration. Here, the increase in terrestrial biosphere carbon both inside and outside of the ice sheet areas, are presumed to reflect the decrease in soil respiration rate due to colder SATs exceeding the decrease in net photosynthesis (i.e. total photosynthesis-respiration) rate due to lower $\mathrm{CO_2}$, SAT and precipitation, as they are mainly driven by soil carbon increases. In most previous model- and observational data-based studies it is conversely suggested that the reduced photosynthesis effect due to climate and $\mathrm{CO_2}$ changes outcompetes the reduced respiration effect on a global scale. In O'ishi and Abe-Ouchi (2013) for example, the terrestrial carbon that would be gained if ice sheet carbon was preserved rather than destroyed (383 PgC) is smaller than the amount of carbon that is lost in response to the LGM climate and $\mathrm{CO_2}$ changes (502 PgC).

Although not evaluated directly, it is likely that similar ice sheet/non-ice sheet terrestrial carbon proportions than in $\mathrm{ENS_{16}}$ are found in $\mathrm{ENS_{104}}$ and $\mathrm{ENS_{315}}$ because of the similar climate change distributions in all three instances (see earlier sections). Although not shown here, the spatial distribution of $\Delta\mathrm{TerrC}$ in $\mathrm{ENS_{16}}$ is also similar to that of the $\mathrm{ENS_{104}}$ (and $\mathrm{ENS_{315}}$) mean. The spatial distribution of $\Delta\mathrm{TerrC}$ in $\mathrm{ENS_{104}}$ is shown in Fig. 11 and compared against observations.

The largest increases in terrestrial carbon (≥ 20 kgC $\mathrm{m^{-2}}$) are found in North America and Europe/western Asia, both within and south of the Laurentide and Eurasian ice sheet margins (Fig. 11). Regions with smaller but still relatively large (≥ 10 kgC $\mathrm{m^{-2}}$) increases include the Andes and Patagonia regions, the southern tip of the African continent, eastern north Siberia and the grid cells just south of the Tibetan plateau. The largest LGM decreases in terrestrial carbon (≥ 10 kgC $\mathrm{m^{-2}}$) conversely tend to be found in northwest North America, Beringia and the Tibetan plateau region. Other regions with relatively large (≥ 5 kgC $\mathrm{m^{-2}}$) decreases include equatorial Africa and the deserts in central Asia. Everywhere else the LGM terrestrial carbon density increases by between 0 and 10 kgC $\mathrm{m^{-2}}$. Comparison against paleoecological reconstruction studies (Crowley et al., 1995) suggests that the simulated terrestrial carbon changes within the Laurentide and Eurasian ice sheet areas are of the wrong sign, except in northwest North America, since these studies assume the complete destruction of vegetation and soils in ice sheet areas. Discrepancies between the ENS_{104} and observations further arise from the rainforest regions, where the ensemble mean predicts terrestrial biosphere carbon density changes between -5 and 10 kgC m^{-2}, well above observed changes of $\sim$ -23 kgC m^{-2}. It is important to note, however, that as suggested in Zeng (2007), the rate of decomposition of soil carbon at the LGM may have been slower than assumed in pollen data-based studies. The largest increases in terrestrial carbon density ($\sim$ 40 kgC m^{-2}) produced by the ensemble mean are comparable to those found in areas with permafrost growth (Zimov et al., 2006). However, the peaks are potentially misplaced, being located within and south of the Laurentide and Eurasian ice sheet covered areas, rather than in eastern Siberia and Alaska. Alternatively, terrestrial carbon increases in eastern Siberia and Alaska are simply underestimated in the ensemble mean and large increases in terrestrial carbon indeed took place within the ice sheet areas during glacial periods.

The highly negative LGM terrestrial carbon changes in northwest North America and adjacent Beringia are likely caused by precipitation decreasing comparatively more than SAT, and causing the decrease in photosynthesis to exceed the decrease in soil respiration. However, it is also noteworthy that, although not shown here, the regions with the largest decreases in terrestrial carbon density, namely northwest North America, Beringia and the Tibetan plateau area, are also the regions with the largest terrestrial carbon densities in the preindustrial simulations. We further, note that in the preindustrial ENS_{315} mean, the Tibetan soil carbon peak is overestimated and the North American soil carbon peak misplaced, compared to observations. We attribute the first discrepancy to the lack of soil weathering in the model and the inclusion of land use effects in the observational data-based estimate (Holden et al., 2013b; Williamson et al., 2006). The second discrepancy is attributed to the lack of explicit representation of permafrost and the absence of moisture control on soil respiration.

Table 5. Ice sheet and non-ice sheet terrestrial carbon stocks. Columns 2 and 5 show the amount of carbon stored in ice sheet areas during the preindustrial and LGM periods respectively. Column 3 is the difference between the two inventories. Column 4 is the change in ice sheet carbon expressed as percentage of the total LGM terrestrial carbon change. Column 6 is the LGM change in carbon outside of the ice sheets.

EM	PRE ice sheet	LGM-PRE ice sheet	% LGM-PRE Total land	LGM Burial	LGM-PRE non-ice sheet
442	456	117	51	573	111
873	896	444	29	1341	1089
511	677	262	32	939	567
99	372	33	20	405	130
871	404	149	26	553	425
786	502	131	21	633	486
107	540	86	22	626	310
701	549	161	36	710	283
801	707	275	39	982	423
219	312	6	16	318	-34
694	389	95	30	484	227
623	697	181	36	879	319
522	713	210	28	923	531
863	408	73	16	480	380
478	573	165	41	739	233
837	784	395	33	1179	796

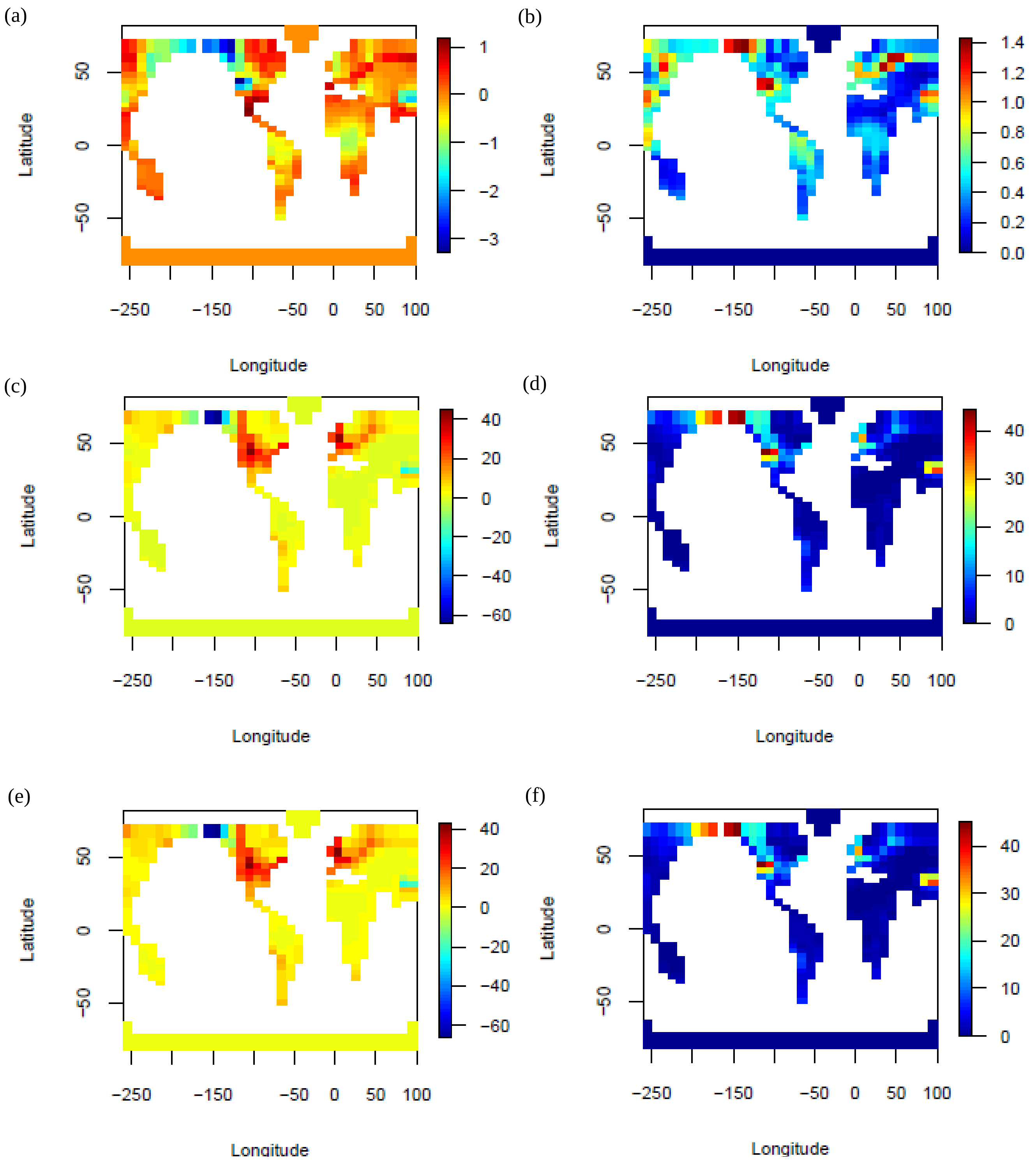

Fig. 11. LGM vegetation (a-b), soil (c-d) and total terrestrial carbon changes (e-f) ENS_{104} mean (left) and standard deviation (right). Units are kgC m^{-2}.

3.2.3 Ocean primary productivity

The ENS_{104} mean LGM total POC export flux anomaly (ΔPOC_{exp}) is -0.19 $\pm$ 1 PgC yr^{-1} and the range is -2.57 to 2.56 PgC yr^{-1}, roughly consistent with previous model-based estimates (e.g. Brovkin et al., 2002; Bopp et al., 2003; Brovkin et al., 2007; Chikamoto et al., 2012; Palastanga et al., 2013; Schmittner and Somes, 2016; Buchanan et al., 2016) (Fig. 12). The POC flux decreases in ENS_{315} and ENS_{16} tend to be smaller and larger respectively. ΔPOC_{exp} is positively correlated with $\Delta\psi_{max}$ (r = 0.72 and 0.79) and negatively correlated with $\Delta\psi_{min}$ (r = -0.62 and -0.58) in both ENS_{104} and ENS_{315}. The correlations potentially suggest that decreasing AMOC strength and increasing AABW production lead to decreasing POC export. One possible mechanism is enhanced deep ocean stratification due to increasing AABW formation leading to not only more efficient trapping of DIC at depth (see above), but also nutrients and therefore reduced availability in the euphotic zone. All else held constant, a weaker and shallower AMOC cell would also inhibit the transfer of nutrients from the deep ocean to the surface. A negative correlation can additionally be found between ΔPOC_{exp} and ΔSIA (r = -0.55 and -0.6), probably because no primary production occurs beneath the sea ice surface and increasing sea ice area at the LGM therefore leads to decreasing POC export flux. This would also explain the largest ENS_{104} mean decreases in POC export flux coinciding with increases in sea ice fraction (Fig. 13).

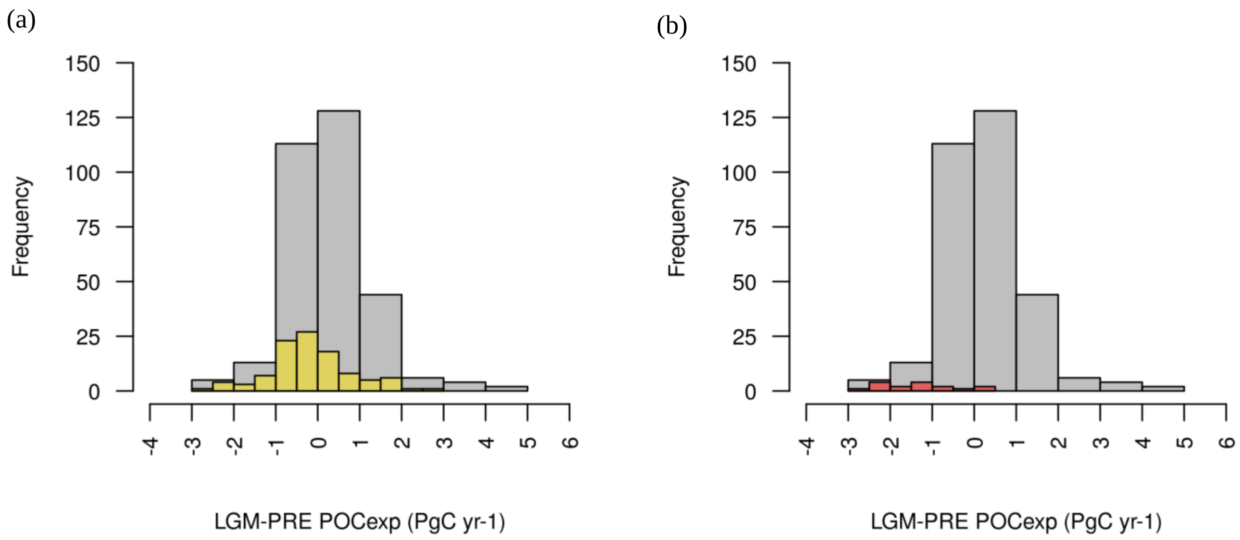

Fig. 12. LGM change in POC export flux (a-b) distributions.

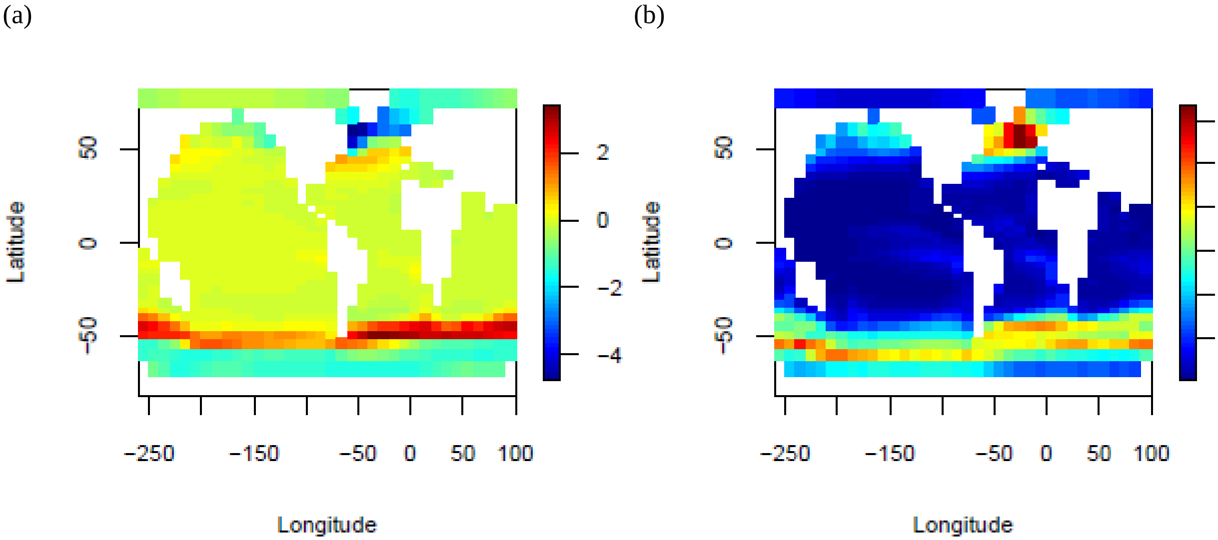

Fig. 13. LGM surface POC export flux change (molC m^{-2} yr^{-1}) ENS_{104} mean (a) and standard deviation (b).

The largest LGM PGACF ensemble *increases* in POC export flux conversely occur at around 50 °S, roughly in front of the Antarctic sea ice margins. Increases in POC export are also simulated close to the North Pacific and Atlantic sea ice margins, as well as in the eastern equatorial Pacific and the southwest Atlantic upwelling region. The sea ice margin POC export flux increases are likely caused by the advection of unutilised nutrients from underneath the sea ice. However, they may additionally be caused by the enhanced iron availability from the increased supply of aeolian dust, particularly in the Southern Ocean and North Pacific since these are strongly limited by iron (Ridgwell et al., 2007). Iron fertilization may also explain the increases in POC export flux in the eastern equatorial Pacific and in the southwest Atlantic upwelling region. Comparison against observations suggests that the ensemble mean POC flux changes immediately north, and south of the Antarctic sea ice margins align with observations of increased and reduced marine productivity in the Subantarctic (~45 to 60 °N) and Southern Ocean respectively (Kohfeld et al., 2005; Kohfeld et al., 2013; Jaccard et al., 2013; Martínez-García et al., 2014). The simulated decreases in export flux in the Arctic and subarctic Atlantic (i.e. above ca. 50 °N), and the increases in export flux immediately south of 50°N are also in agreement with previous reconstructions (Kohfeld et al., 2005; Radi and de Vernal, 2008).The mostly lower LGM export fluxes at the equator and in the South Atlantic are conversely inconsistent with the observational data of Kohfeld et al., (2005). The decreases may be caused by the increases in productivity in HNLC regions reducing the phosphate (the other limiting nutrient in GENIE-1 besides iron) availability for photosynthesis in other regions. They may additionally be due to the model not simulating enhanced nutrient inventories in response to enhanced weathering or reduced shallower water deposition of organic matter. The model also does not vary wind speed which may have resulted in stronger tropical upwelling in the Atlantic at the LGM. The evidence is more ambiguous (or missing) for the

Pacific (Jaccard et al., 2010; Kohfeld and Chase, 2011; Kohfeld et al., 2005; Costa et al., 2016) and Indian Oceans (Kohfeld et al., 2005; Singh et al., 2011) and is therefore not discussed in more detail here.

3.2.4 Carbonate weathering and shallow water deposition

The ENS_{104} mean glacial weathering factor (GWS) is 1.16 $\pm$ 0.24 (corresponding to a percentage change in the land to ocean bicarbonate flux (%LOC) of 38.67), and the range is 0.52 to 1.5 (corresponding to a %LOC between -49.33 and 50). (Fig. 14). The GWS in ENS_{104} tends to be larger than in ENS_{315} and smaller than in ENS_{16}. There is also a negative correlation between GWS and $\Delta\mathrm{CO}_2$ (r = -0.52) in ENS_{315}, suggesting that increasing the input of bicarbonate to the ocean leads to a decrease in CO_2 by raising the inventories of ALK and DIC in a 2:1 ratio. In ENS_{104}, however, r is below the 0.05 significance level, suggesting that it is less important.

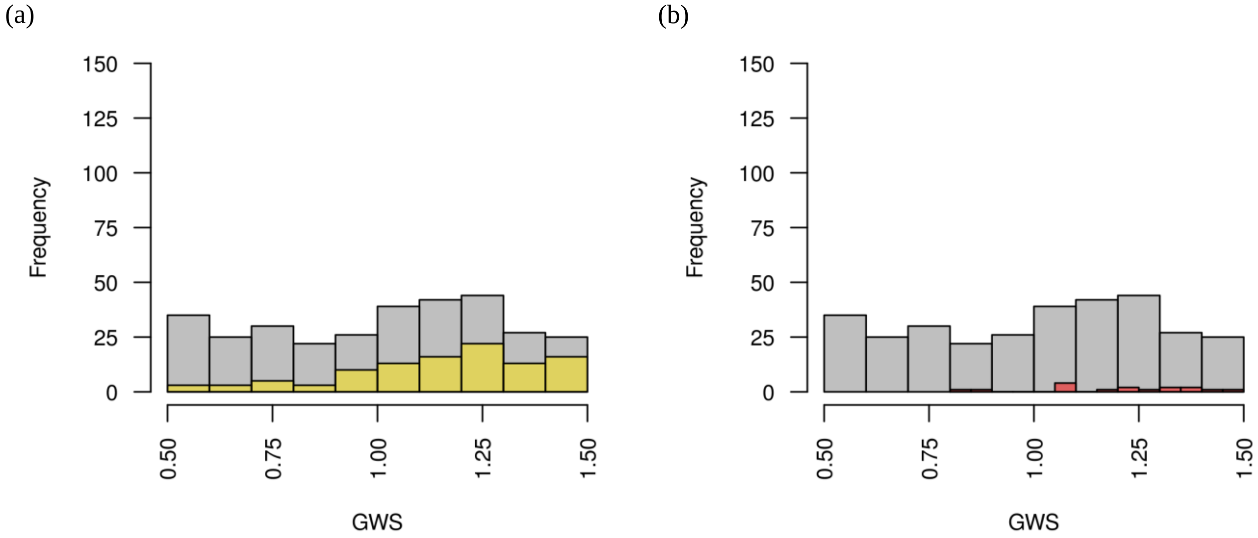

Fig. 14. GWS (a-b) distributions.

3.2.5 Deep-sea carbonate burial

The ENS_{104} mean global deep-sea $CaCO_3$ burial flux anomaly ($\Delta CaCO3_{bur}$) is 0.036 ± 0.045 PgC yr^{-1} and the range is -0.098 to 0.139 PgC yr^{-1} (Fig. 15). The mean value is ca. 3 times larger than the observed value (Catubig et al., 1998), although the latter still falls within the range of simulated values. $\Delta CaCO3_{bur}$ in ENS_{104} tends to be higher than in ENS_{315}, and lower than in ENS_{16}. It is strongly determined by GWS, as suggested by the positive correlation (r = 0.88 and 0.9) between the two, in both ENS_{104} and ENS_{315}. Increasing %LOC should indeed cause the $CaCO_3$ burial flux to increase as increasing ALK means the deep ocean CO_3^{2-} will eventually increase, causing the saturation horizon to fall and allowing $CaCO_3$ to accumulate over greater areas (which are now exposed to undersaturated waters) (Sigman and Boyle, 2000). The input of ALK to the surface ocean will also increase the rate of $CaCO_3$ export production (which will in turn increase the sediment deposition flux of $CaCO_3$) since as discussed in Chikamoto et al. (2008), the latter is proportional to the production rate of POC (which is equal to the POC export flux), together with the sea surface saturation state with respect to $CaCO_3$, in GENIE-1. There is indeed also a positive correlation between %LOC and the global change in $CaCO_3$ export (r = 0.27 and 0.4), and between the latter and $\Delta CaCO3_{bur}$ (r = 0.34 and 0.45) in both ENS_{104} and ENS_{315}.

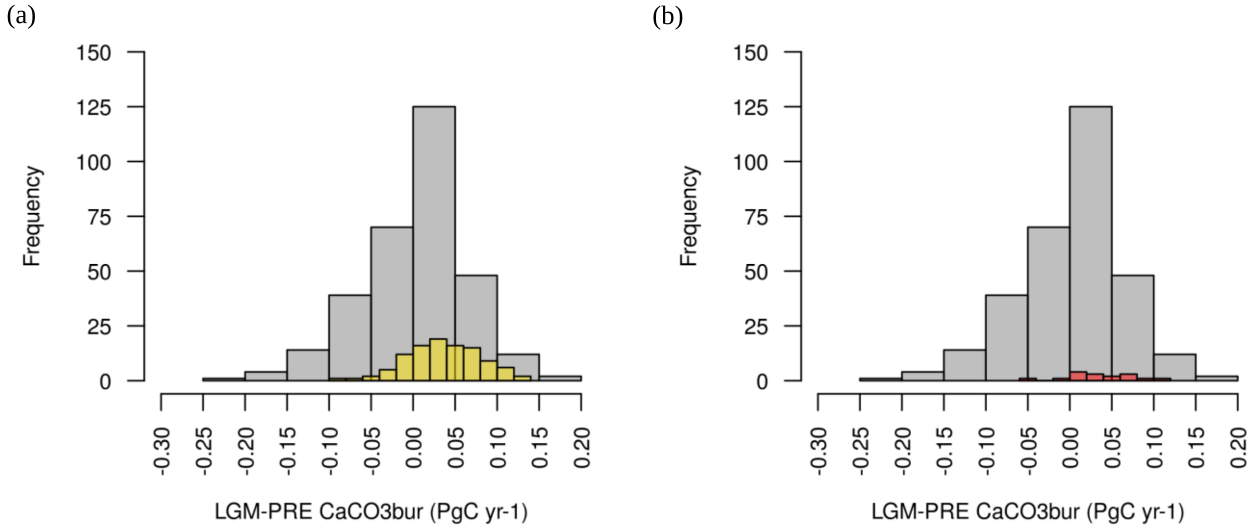

Fig. 15. LGM change in deep sea sediment $CaCO_3$ burial flux (a-b) distributions.

The ENS_{104} mean spatial distribution of $\Delta CaCO3_{bur}$ is shown in Fig. 16. Relatively large increases in burial flux ($\geq 0.5 \times 10^{-5}$ mol cm^{-2} yr^{-1}) can be found at around 50 °S, in the North Pacific, and to a lesser extent the North Atlantic. In other regions, the burial flux is significantly lower or negative, with the largest losses ($\leq$ -0.5 $\times 10^{-5}$ mol cm^{-2} yr^{-1}) occurring the North Atlantic and arctic regions. The only exception is the western North Atlantic which exhibits a large in burial. A comparison of the results against the reconstructions of Catubig et al., 1998 is somewhat difficult as the coverage is poor but overall $CaCO_3$ burial was higher in the North Atlantic and the Pacific, and lower in the tropical and South Atlantic, and the Indian and Southern Ocean.

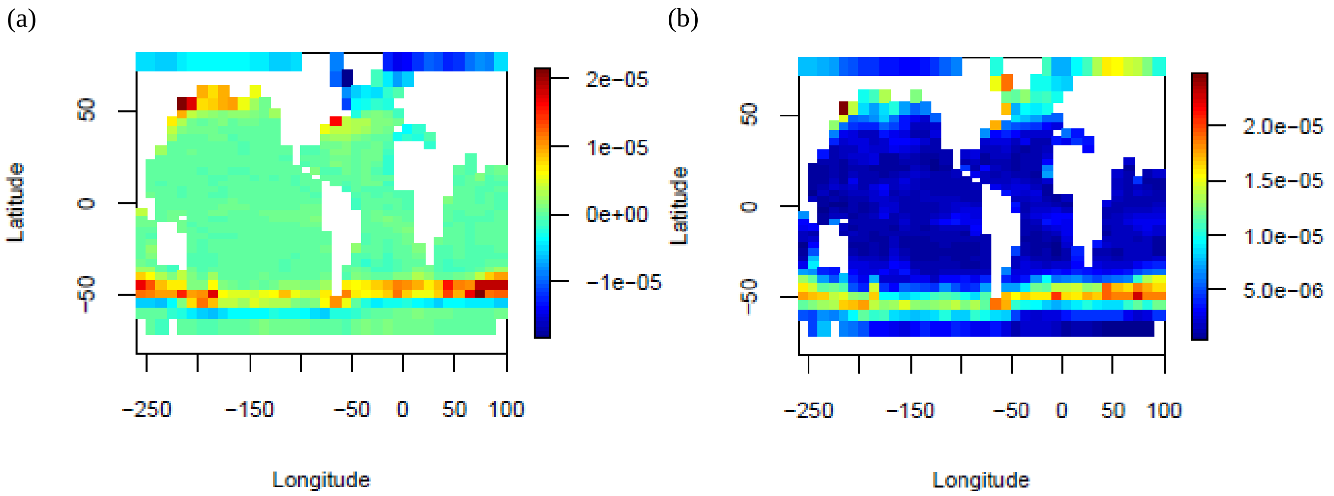

Fig. 16. LGM deep sea $CaCO_3$ burial rate change (mol cm^{-2} yr^{-1}) ENS_{104} mean (a) and standard deviation (b).

3.2.6 Other paleo proxies

To further evaluate the sign and magnitude of our simulated LGM changes, and in particular ΔTerrC, a key future test would be to add carbon isotopes into GENIE-1's terrestrial biosphere carbon module and re-run the ENS_{104} LGM simulations with $\Delta^{14}C_{atm\ (DIC)}$ and $\delta^{13}C_{atm\ (DIC)}$ spun up. As shown in Table 4, a frequent argument for a lower glacial terrestrial carbon inventory is the reconstructed mean glacial ocean $\delta^{13}C$ value of ca. 0.35‰ lower than present due to the fact that plants discriminate against ^{13}C during photosynthesis. In our simulations conversely, it follows that the increase in glacial terrestrial carbon inventory would have resulted in an *increase* in ocean $\delta^{13}C$. However, other processes such as reduced marine productivity, lower SSTs (Schmitt et al., 2012) and greater sea ice area (Stephen and Keeling, 2000) may have counteracted at least some of this increase. Increasing LGM $CaCO_3$ weathering flux would have conversely raised ocean $\delta^{13}C$ although our model does not account for changes in the organic carbon weathering flux, which if increased would result in a decrease in $\delta^{13}C$. Wallmann (2014) attribute most of the observed LGM ocean $\delta^{13}C$ decrease to enhanced weathering and reduced deposition of organic carbon at continental margins due to lower sea levels. Menviel et al. (2015) have also shown that weaker surface winds can contribute to a lower ocean $\delta^{13}C$ while these are held fixed in our model. It has further been argued that enhanced glacial carbonate ion concentrations may have reduced the $\delta^{13}C$ in foraminera shells without altering mean ocean $\delta^{13}C$ (Lea et al., 1999).

As discussed in Zeng (2003) the glacial increase in terrestrial carbon inventory may also potentially explain transient trends in the glacial-interglacial atmospheric $\delta^{13}C$ record, such as the increase in atmospheric $\delta^{13}C$ over the glaciation, and the decrease of about 0.3 ‰ at the beginning of the deglaciation (Smith et al., 1999). Another feature of the deglacial record, namely the rise in $\delta^{13}C_{atm}$ between ca. 12 and 7 kyr BP, is in turn attributed to increasing SSTs and terrestrial biosphere regrowth on previously ice-covered areas. A more common explanation for the deglacial $\delta^{13}C_{atm}$ variation, which resembles the letter W, is conversely that the beginning of the pattern was caused by the release of old carbon from the deep ocean while the end of the pattern was largely due to terrestrial biosphere regrowth. The middle section of the W, characterised by subdued variation in $\delta^{13}C_{atm}$, is attributed to abrupt climate changes (Schmitt et al., 2012). More recently, however, it has also been suggested that the deglacial decrease in $\delta^{13}C_{atm}$ at ca. 17.5 kyr BP may be caused at least partly by the demise of iron-stimulated Southern Ocean biological productivity (Fischer et al., 2015) and the release of carbon from thawing permafrost (Crichton et al., 2016). A better test, therefore, would be for the ENS_{104} ensemble members to not only simulate LGM-PRE $\delta^{13}C_{atm}$ but also the transient changes in $\delta^{13}C_{atm}$ over the deglaciation. A further test would be to compare the simulated spatial distribution of $\delta^{13}C$ with observations (e.g. Menviel et al., 2017).

Another frequent but more indirect argument for a lower glacial terrestrial carbon inventory is the deglacial drop in atmospheric $\Delta^{14}C$, which is typically attributed to the release of old ocean carbon accumulated over the previous glacial period. Zeng (2007) and others (e.g. Zech, 2012) conversely propose that it is caused by the release of very old, and therefore ^{14}C-depleted, carbon from the terrestrial biosphere. More recent higher resolution records of deglacial $\Delta^{14}C$ and atmospheric CO_2 (e.g. Durand et al., 2013 in Köhler et al., 2014; Marcott et al., 2014) have, however, so far not been discussed by the enhanced glacial terrestrial carbon inventory studies. Another challenge is that a terrestrial biosphere-induced early deglacial decrease in atmospheric $\Delta^{14}C$ would have also led to a decrease in ocean $\Delta^{14}C$ and this is yet to be reconciled with ocean $\Delta^{14}C$ data. Studies so far have suggested there was a decrease in deep ocean $\Delta^{14}C$ during the glaciation, corresponding to an increase in ventilation age, and an increase in deep ocean $\Delta^{14}C$ at deglaciation, corresponding to a decrease in ventilation age, and also coinciding with the decrease in atmospheric $\Delta^{14}C$ (Hughen et al., 2006; Skinner et al., 2010; Skinner et al., 2015; de la Fuente et al., 2015; Freeman et al., 2015). With a reduced deep ocean ventilation at the LGM, it is assumed that the carbon sequestration capacity of the ocean was enhanced, and that the magnitude and spread of these changes resulted in a global increase rather than decrease in ocean carbon.

A potential limitation, however, with the use of ocean $\Delta^{14}\mathrm{C}$ to infer larger LGM ocean carbon inventory pools is the presence of $\Delta^{14}\mathrm{C}_{\mathrm{DIC}}$ which indicate no change in ventilation age, or conversely an increase (Broecker and Barker, 2007; Broecker and Clark, 2010; Cléroux et al., 2010; Lund et al., 2011), and processes besides water mass aging which may have contributed to decreasing glacial $\Delta^{14}\mathrm{C}_{\mathrm{DIC}}$ such as decreasing atmospheric $^{14}\mathrm{C}$ production rate, increased weathering of $^{14}\mathrm{C}$-depleted $\mathrm{CaCO_3}$, input of $^{14}\mathrm{C}$-depleted carbon from the mantle and inaccurate estimation of surface ocean reservoir age (Broecker and Barker, 2007; Lund et al., 2011; Wagner and Hendy, 2015). The feasibility of a large extremely $^{14}\mathrm{C}$-depleted deep ocean carbon reservoir has also been contested in terms of atmospheric $\mathrm{CO_2}$, deep ocean oxygen (namely the absence of large-scale anoxia) and $\mathrm{CaCO_3}$ depth constraints (Hain et al., 2011), and from a dynamical standpoint (Broecker and Clark, 2010). Another strong future test would therefore be for ENS_{104} to simulate spatially resolved LGM ocean $\Delta^{14}\mathrm{C}$, as well as the changes in atmospheric $\Delta^{14}\mathrm{C}$ over the deglaciation.

Finally, we have shown that decreasing LGM atmospheric $\mathrm{CO_2}$ in our ensemble tends to be accompanied by decreasing POC export production, which all else held constant would result in an increase in deep ocean oxygenation – a feature which we have not assessed. Proxy records to date conversely tend to indicate that there was a decrease, not an increase, in deep ocean oxygen concentration (Jaccard et al., 2016). When observed over sufficiently large areas, the latter supports the presence of an enhanced ocean carbon inventory as deoxygenation can be explained by reduced ocean ventilation (the sole input of oxygen is from the ocean surface) (Wagner and Hendy, 2015). As discussed above, the reduced ventilation is in turn assumed to have led to the accumulation of a significant amount of DIC in the ocean interior. Thus, explaining the lower deep ocean oxygen concentrations without having to reduce ocean ventilation as extensively as suggested by previous studies would as a minimum likely require LGM export production to have increased rather than decreased (assuming the enhanced POC export production does not automatically result in an increase in glacial ocean carbon inventory). Alternatively, it may be possible to increase deep ocean oxygen consumption by increasing organic matter at depth but keeping the surface POC export flux constant. This would require adding processes such as increasing remineralisation depth with decreasing ocean temperature and increasing ballasting into our model (Kohfeld and Ridgwell, 2009; Menviel et al., 2012). We also note that including missing processes affecting the ocean biological pump such as increased oceanic $\mathrm{PO_4}$ inventory could potentially result in a net increase in LGM POC export, helping lower oxygen concentrations. However, this would then make reconciliation of our positive $\Delta\mathrm{TerrC}$ with the observed negative LGM ocean $\delta^{13}\mathrm{C}$ more difficult.

4 Conclusions

We have used an uncertainty-based approach to investigating the LGM atmospheric CO_2 drop by simulating it with a large ensemble of parameter sets, designed to allow for a wide range of large-scale feedback response strengths. Our objective was not to definitely explain the causes of the CO_2 drop but rather explore the range of possible responses. Our investigation also involved simulating the CO_2 drop with the simulated CO_2 feeding back to the simulated climate, which is still relatively rare in LGM atmospheric CO_2 experiments, and the first time it is done with GENIE-1. Moreover, rather than assuming that terrestrial carbon gets destroyed by the LGM ice sheets, we allowed for its gradual burial. This assumption had not yet been implemented in an equilibrium set-up.

Despite our ensemble varying many of the parameters thought to contribute to variability in glacial-interglacial atmospheric CO_2, not all sources of uncertainty could be captured, and this was reflected in our simulated ΔCO_2 distribution. We estimated that up to ~60 ppmv of ΔCO_2 could be attributed to processes not included in our model and error in our process representations. As a result, we treated simulations with ΔCO_2 between ~-90 and -30 ppmv as "equally plausible", and focused on describing the physical and biogeochemical changes seen in this subset, as well as their linkages to ΔCO_2. We found the range of responses to be large, including the presence of five different ways of achieving a plausible ΔCO_2 in terms of the sign of individual carbon reservoir changes. However, several dominant changes could be detected. Namely: the LGM atmospheric CO_2 decrease tended to predominantly be associated with decreasing SSTs, increasing sea ice area, a weakening of the AMOC, a strengthening of the AABW cell in the Atlantic Ocean, a decreasing ocean biological productivity, an increasing $CaCO_3$ weathering flux and an increasing deep-sea $CaCO_3$ burial flux. The majority of our simulations also predicted an increase in terrestrial carbon, coupled with a decrease in ocean and an increase in lithospheric carbon. The increase in terrestrial carbon, which is uncommon in LGM simulations, was attributed to our choice to preserve rather than destroy ice sheet carbon, as well as the fact that the latter increased rather than decreased in response to climate forcings. If most of the carbon that was present in ice sheet areas at the end of the preindustrial runs had been lost to climate forcings, it would not matter much whether the remaining stocks had been destroyed or preserved. From the literature, it is not clear how much of the carbon in ice sheet areas is thought to have been lost strictly in response to ice sheet "bulldozing" versus climate impacts.

An initial comparison of the dominant changes with observations and paleo-proxies suggested broad agreement. However, a comparison against carbon isotope data would be needed to more robustly determine agreement between our model results and empirical data. Another useful future research endeavour would be to investigate the relationships between the simulated changes and ensemble parameters, in order to help isolate the individual mechanisms that directly, or indirectly, cause atmospheric CO_2 to change.

Acknowledgements

This work made use of the Darwin Supercomputer of the University of Cambridge High Performance Computing Service (HPCS). K.M.S. Kemppinen thanks staff at HPCS for their technical support, and Antara Banerjee and Alex Archibald for help with R This manuscript was greatly improved by comments from an anonymous reviewer.

References

Adams, J. M. and Faure, H.: A new estimate of changing carbon storage on land since the last glacial maximum, based on global land ecosystem reconstruction, Glob. Planet. Change, 16–17, 3–24, doi:10.1016/S0921-8181(98)00003-4, 1998.

Adkins, J. F., Mcintyre, K. and Schrag, D. P.: The Salinity, Temperature, and d18O of the Glacial Deep Ocean, Science, 298(November), 1769–1773, doi:10.1126/science.1076252, 2002.

Alder, J. R. and Hostetler, S. W.: Global climate simulations at 3000-year intervals for the last 21 000 years with the GENMOM coupled atmosphere-ocean model, Clim. Past, 11(3), 449–471, doi:10.5194/cp-11-449-2015, 2015.

Allen, K. A., Sikes, E. L., Hönisch, B., Elmore, A. C., Guilderson, T. P., Rosenthal, Y. and Anderson, R. F.: Southwest Pacific deep water carbonate chemistry linked to high southern latitude climate and atmospheric CO2 during the Last Glacial Termination, Quat. Sci. Rev., 122, 180–191, doi:10.1016/j.quascirev.2015.05.007, 2015.

Anderson, R. F., Ali, S., Bradtmiller, L. I., Nielsen, S. H. H., Fleisher, M. Q., Anderson, B. E. and Burckle, L. H.: Wind-Driven Upwelling in the Southern Ocean and the Deglacial Rise in Atmospheric CO2, Science, 323(5920), 1443–1448, doi:10.1126/science.1167441, 2009.

Annan, J. D. and Hargreaves, J. C.: A new global reconstruction of temperature changes at the Last Glacial Maximum, Clim. Past, 9(1), 367–376, doi:10.5194/cp-9-367-2013, 2013.Annan, J. D. and Hargreaves, J. C.: Efficient identification of ocean thermodynamics in a physical/biogeochemical ocean model with an iterative Importance Sampling method, Ocean Model., 32(3–4), 205–215, doi:10.1016/j.ocemod.2010.02.003, 2010.

Ballarotta, M., Falahat, S., Brodeau, L. and Döös, K.: On the glacial and interglacial thermohaline circulation and the associated transports of heat and freshwater, Ocean Sci., 10(6), 907–921, doi:10.5194/os-10-907-2014, 2014.

Bartlein, P. J., Harrison, S. P., Brewer, S., Connor, S., Davis, B. A. S., Gajewski, K., Guiot, J., Harrison-Prentice, T. I., Henderson, A., Peyron, O., Prentice, I. C., Scholze, M., Seppä, H., Shuman, B., Sugita, S., Thompson, R. S., Viau, A. E., Williams, J. and Wu, H.: Pollen-based continental climate reconstructions at 6 and 21 ka: A global synthesis, Clim. Dyn., 37(3), 775–802, doi:10.1007/s00382-010-0904-1, 2011.

Berger, A.: Long-term variations of daily insolation and quaternary climatic changes, J. Atmos. Sci. 35(12), 2362–2367, 1978.

Böhm, E., Lippold, J., Gutjahr, M., Frank, M., Blaser, P., Antz, B., Fohlmeister, J., Frank, N., Andersen, M. B. and Deininger, M.: Strong and deep Atlantic meridional overturning circulation during the last glacial cycle, Nature, 517(7534), 73–76, doi:10.1038/nature14059, 2015.

Bopp, L., Kohfeld, K. E., Le Quéré, C. and Aumont, O.: Dust impact on marine biota and atmospheric CO2 during glacial periods, Paleoceanography, 18(2), 1046, dio:10.1029/2002PA000810, doi:10.1029/2002PA000810, 2003.

Bouttes, N., Paillard, D. and Roche, D. M.: Impact of brine-induced stratification on the glacial carbon cycle, Clim. Past, 6(5), 575–589, doi:10.5194/cp-6-575-2010, 2010.

Bouttes, N., Paillard, D., Roche, D. M., Brovkin, V. and Bopp, L.: Last Glacial Maximum CO2 and δ13C successfully reconciled, Geophys. Res. Lett., 38(2), Citation No. L02705, doi:10.1029/2010gl044499, 2011.

Broecker, W. and Barker, S.: A 190‰ drop in atmosphere's Δ14C during the "Mystery Interval" (17.5 to 14.5 kyr), Earth Planet. Sci. Lett., 256(1–2), 90–99, doi:10.1016/j.epsl.2007.01.015, 2007.

Broecker, W. and Clark, E.: Search for a glacial-age 14C-depleted ocean reservoir, Geophys. Res. Lett., 37(13), doi:10.1029/2010GL043969, 2010.

Brovkin, V. and Ganopolski, A.: The role of the terrestrial biosphere in CLIMBER-2 simulations of the last glacial CO2 cycles. Nova Act Lc NF, 121, 43-47, 2015.

Brovkin, V., Hofmann, M., Bendtsen, J. and Ganopolski, A.: Ocean biology could control atmospheric delta C-13 during glacial-interglacial cycle, Geochemistry Geophys. Geosystems, 3, 22, doi:1027\r10.1029/2001gc000270, 2002.

Brovkin, V., Ganopolski, A., Archer, D. and Rahmstorf, S.: Lowering of glacial atmospheric CO2 in response to changes on oceanic circulation and marine biogeochemistry, Paleoceanography, 22(4), doi:10.1029/2006PA001380, 2007.

Brovkin, V., Ganopolski, A., Archer, D. and Munhoven, G.: Glacial CO 2 cycle as a succession of key physical and biogeochemical processes, Clim. Past, 8(1), 251–264, doi:10.5194/cp-8-251-2012, 2012.

Buchanan, P. J., Matear, R. J., Lenton, A., Phipps, S. J., Chase, Z. and Etheridge, D.: The simulated climate of the Last Glacial Maximum and insights into the global carbon cycle, Clim. Past Discuss., 11(2), 1–45, doi:10.5194/cp-2016-73, 2016.

Catubig, N. R., Archer, D. E., Francois, R., DeMenocal, P., Howard, W. and Yu, E. F.: Global deep-sea burial rate of calcium carbonate during the Last Glacial Maximum, Paleoceanography, 13(3), 298–310, doi:10.1029/98PA00609, 1998.

Chikamoto, M. O., Matsumoto, K. and Ridgwell, A.: Response of deep-sea CaCO3 sedimentation to Atlantic meridional overturning circulation shutdown, J. Geophys. Res. Biogeosciences, 113(3), doi:10.1029/2007JG000669, 2008.

Chikamoto, M. O., Abe-Ouchi, A., Oka, A., Ohgaito, R. and Timmermann, A.: Quantifying the ocean's role in glacial CO2 reductions, Clim. Past, 8(2), 545–563, doi:10.5194/cp-8-545-2012, 2012.

Ciais, P., Tagliabue, A., Cuntz, M., Bopp, L., Scholze, M., Hoffmann, G., Lourantou, A., Harrison, S. P., Prentice, I. C., Kelley, D. I., Koven, C. and Piao, S. L.: Large inert carbon pool in the terrestrial biosphere during the Last Glacial Maximum, Nat. Geosci., 5(1), 74–79, doi:10.1038/ngeo1324, 2012.

Ciais, P., Sabine, C., Bala, G., Bopp, L., Brovkin, V., Canadell, J., Chhabra, A., DeFries, R., Galloway, J., Heimann, M., Jones, C., Quéré, C. Le, Myneni, R. B., Piao, S. and Thornton, P.: The physical science basis. Contribution of working group I to the fifth assessment report of the intergovernmental panel on climate change, Chang. IPCC Clim., 465–570, doi:10.1017/CBO9781107415324.015, 2013.

Cléroux, C., deMenocal, P. and Guilderson, T.: Deglacial radiocarbon history of tropical Atlantic thermocline waters: Absence of CO2 reservoir purging signal, Quat. Sci. Rev., 30(15–16), 1875–1882, doi:10.1016/j.quascirev.2011.04.015, 2011.

Colbourn, G.: Weathering effects on the carbon cycle in an Earth System Model, Ph.D. thesis, School of Environmental Sciences, University of East Anglia, United Kingdom, 2011.

Costa, K. M., McManus, J. F., Anderson, R. F., Ren, H., Sigman, D. M., Winckler, G., Fleisher, M. Q., Marcantonio, F. and Ravelo, A. C.: No iron fertilization in the equatorial Pacific Ocean during the last ice age, Nature, 529(7587), 519–522, doi:10.1038/nature16453, 2016.

Crichton, K. A., Bouttes, N., Roche, D. M., Chappellaz, J. and Krinner, G.: Permafrost carbon as a missing link to explain CO 2 changes during the last deglaciation, Nat. Geosci., 9(9), 683–686, doi:10.1038/ngeo2793, 2016.

Crocket, K.C., Vance, D., Foster, G.L., Richards, D.A. and Tranter, M.:Continental weathering fluxes during the last glacial/interglacial cycle: insights from the marine sedimentary Pb isotope record at Orphan Knoll, NW Atlantic, Quaternary Sci Rev 38: 89-99. Doi: 10.1016/j.quascirev.2012.02.004, 2012.

Crowley, T. J.: Ice Age terrestrial carbon changes revisited, Global Biogeochem. Cycles, 9(3), 377–389, doi:10.1029/95GB01107, 1995.

De La Fuente, M., Skinner, L., Calvo, E., Pelejero, C. and Cacho, I.: Increased reservoir ages and poorly ventilated deep waters inferred in the glacial Eastern Equatorial Pacific, Nat. Commun., 6, doi:10.1038/ncomms8420, 2015.

Doney, S. C., Lindsay, K., Fung, I. and John, J.: Natural variability in a stable, 1000-yr global coupled climate-carbon cycle simulation, J. Clim., 19(13), 3033–3054, doi:10.1175/JCLI3783.1, 2006.

Durand, N., Deschamps, P., Bard, E., Hamelin, B., Camoin, G., Thomas, A. L., Henderson, G. M., Yokoyama, Y. and Matsuzaki, H.: Comparison of 14C and U-Th Ages in Corals from IODP #310 Cores Offshore Tahiti, Radiocarbon, 55(4), 1947–1974, doi:10.2458/azu_js_rc.v55i2.16134, 2013.

Edwards, N. R. and Marsh, R.: Uncertainties due to transport-parameter sensitivity in an efficient 3-D ocean-climate model, Clim. Dyn., 24(4), 415–433, doi:10.1007/s00382-004-0508-8, 2005.

Ferrari, R., Jansen, M. F., Adkins, J. F., Burke, A., Stewart, A. L. and Thompson, A. F.: Antarctic sea ice control on ocean circulation in present and glacial climates, Proc. Natl. Acad. Sci., 111(24), 8753–8758, doi:10.1073/pnas.1323922111, 2014.

Fischer, H. , Schmitt, J. , Schneider, R. , Eggleston, S. , Joos, F. , Bauska, T. K. , Marcott, S. A. , Brook, E. J. , Köhler, P. and Chappellaz, J.: Latest Insights into Past Carbon Cycle Changes from CO2 and δ13Catm , Nova Act Lc, 121 (408), 59-63, 2015.

Foster, G. L. and Vance, D.: Negligible glacial-interglacial variation in continental chemical weathering rates, Nature, 444(7121), 918–921, doi:10.1038/nature05365, 2006.

Franzen, L. G.: Are wetlands the key to the ice-age cycle enigma, Ambio, 23(4), 300–308, 1994.

Franzén, L.G. and Cropp, R.A.: The Peatland/ice age Hypothesis revised, adding a possible glacial pulse trigger. Geogr. Ann., 89 A (4): 301–330, 2007.

Freeman, E., Skinner, L. C., Tisserand, A., Dokken, T., Timmermann, A., Menviel, L. and Friedrich, T.: An Atlantic-Pacific ventilation seesaw across the last deglaciation, Earth Planet. Sci. Lett., 424, 237–244, doi:10.1016/j.epsl.2015.05.032, 2015.

Gebbie, G.: How much did Glacial North Atlantic Water shoal?, Paleoceanography, 29(3), 190–209, doi:10.1002/2013PA002557, 2014.

Goodwin, P. and Lauderdale, J. M.: Carbonate ion concentrations, ocean carbon storage, and atmospheric CO 2, Global Biogeochem. Cycles, 27(3), 882–893, doi:10.1002/gbc.20078, 2013.

Hain, M. P., Sigman, D. M. and Haug, G. H.: Shortcomings of the isolated abyssal reservoir model for deglacial radiocarbon changes in the mid-depth Indo-Pacific Ocean, Geophys. Res. Lett., 38(4), doi:10.1029/2010GL046158, 2011.

Harrison, K. G.: Role of increased marine silica input on paleo-pCO<inf>2</inf> levels, Paleoceanography, 15(3), 292–298, doi:10.1029/1999PA000427, 2000.

Holden, P. B., Edwards, N. R., Oliver, K. I. C., Lenton, T. M. and Wilkinson, R. D.: A probabilistic calibration of climate sensitivity and terrestrial carbon change in GENIE-1, Clim. Dyn., 35(5), 785–806, doi:10.1007/s00382-009-0630-8, 2010a.

Holden, P. B., Edwards, N. R., Wolff, E. W., Lang, N. J., Singarayer, J. S., Valdes, P. J. and Stocker, T. F.: Interhemispheric coupling, the West Antarctic Ice Sheet and warm Antarctic interglacials, Clim. Past, 6(4), 431–443, doi:10.5194/cp-6-431-2010, 2010b.

Holden, P. B., Edwards, N. R., Müller, S. A., Oliver, K. I. C., Death, R. M. and Ridgwell, A.: Controls on the spatial distribution of oceanic δ13CDIC, Biogeosciences, 10(3), 1815–1833, doi:10.5194/bg-10-1815-2013, 2013a.

Holden, P. B., Edwards, N. R., Gerten, D. and Schaphoff, S.: A model-based constraint on CO2 fertilisation, Biogeosciences, 10(1), 339–355, doi:10.5194/bg-10-339-2013, 2013b.

Houghton, J. T., Jenkins, G. J., Ephraums, J. J.: Climate Change. The IPCC Scientitific Assessment. Cambridge University Press, Cambridge, 1990.

Hughen, K., Southon, J., Lehman, S., Bertrand, C. and Turnbull, J.: Marine-derived 14C calibration and activity record for the past 50,000 years updated from the Cariaco Basin, Quat. Sci. Rev., 25(23–24), 3216–3227, doi:10.1016/j.quascirev.2006.03.014, 2006.

Iglesias-Rodríguez, M. D., Brown, C. W., Doney, S. C., Kleypas, J., Kolber, D., Kolber, Z., Hayes, P. K. and Falkowski, P. G.: Representing key phytoplankton functional groups in ocean carbon cycle models: Coccolithophorids, Global Biogeochem. Cycles, 16(4), 47-1-47–20, doi:10.1029/2001GB001454, 2002.

Jaccard, S. L., Galbraith, E. D., Sigman, D. M. and Haug, G. H.: A pervasive link between Antarctic ice core and subarctic Pacific sediment records over the past 800 kyrs, Quat. Sci. Rev., 29(1–2), 206–212, doi:10.1016/j.quascirev.2009.10.007, 2010.

Jaccard, S. L., Hayes, C. T., Martinez-Garcia, A., Hodell, D. A., Anderson, R. F., Sigman, D. M. and Haug, G. H.: Two Modes of Change in Southern Ocean Productivity Over the Past Million Years, Science, 339(6126), 1419–1423, doi:10.1126/science.1227545, 2013.

Jaccard, S. L., Galbraith, E. D., Martínez-Garciá, A. and Anderson, R. F.: Covariation of deep Southern Ocean oxygenation and atmospheric CO2 through the last ice age, Nature, 530(7589), 207–210, doi:10.1038/nature16514, 2016.

Jones, I. W., Munhoven, G., Tranter, M., Huybrechts, P. and Sharp, M. J.: Modelled glacial and non-glacial HCO3−, Si and Ge fluxes since the LGM: Little potential for impact on atmospheric CO2concentrations and a potential proxy of continental chemical erosion, the marine Ge/Si ratio, Glob. Planet. Change, 33(1–2), 139–153, doi:10.1016/S0921-8181(02)00067-X, 2002.

Joos, F., Gerber, S., Prentice, I. C., Otto-Bliesner, B. L. and Valdes, P. J.: Transient simulations of Holocene atmospheric carbon dioxide and terrestrial carbon since the Last Glacial Maximum, Global Biogeochem. Cycles, 18(2), doi:10.1029/2003GB002156, 2004.

Kim, S.-J., Flato, G. and Boer, G.: A coupled climate model simulation of the Last Glacial Maximum, Part 2: approach to equilibrium, Clim. Dyn., 20(6), 635–661, doi:10.1007/s00382-002-0292-2, 2003.

Kleypas, J. A.: Modeled estimates of global reef habitat and carbonate production since the last glacial maximum, Paleoceanography, 12(4), 533–545, doi:10.1029/97PA01134, 1997.

Kohfeld, K. E.: Role of Marine Biology in Glacial-Interglacial CO2 Cycles, Science, 308(5718), 74–78, doi:10.1126/science.1105375, 2005.

Kohfeld, K. E. and Chase, Z.: Controls on deglacial changes in biogenic fluxes in the North Pacific Ocean, Quat. Sci. Rev., 30(23–24), 3350–3363, doi:10.1016/j.quascirev.2011.08.007, 2011.

Kohfeld, K. E. and Ridgwell, A.: Glacial-Interglacial Variability in Atmospheric CO2, Surf. Ocean. Atmos. Process., 251–286, doi:10.1029/2008GM000845, 2009.

Kohfeld, K. E., Graham, R. M., de Boer, A. M., Sime, L. C., Wolff, E. W., Le Quéré, C. and Bopp, L.: Southern Hemisphere westerly wind changes during the Last Glacial Maximum: Paleo-data synthesis, Quat. Sci. Rev., 68, 76–95, doi:10.1016/j.quascirev.2013.01.017, 2013.

Köhler, P., Knorr, G. and Bard, E.: Permafrost thawing as a possible source of abrupt carbon release at the onset of the Bølling/Allerød, Nat. Commun., 5, doi:10.1038/ncomms6520, 2014.

Lambert, F., Tagliabue, A., Shaffer, G., Lamy, F., Winckler, G., Farias, L., Gallardo, L. and De Pol-Holz, R.: Dust fluxes and iron fertilization in Holocene and Last Glacial Maximum climates, Geophys. Res. Lett., 42(14), 6014–6023, doi:10.1002/2015GL064250, 2015.

Lea, D. W., Bijma, J., Spero, H. J. and Archer, D.: Implications of a Carbonate Ion Effect on Shell Carbon and Oxygen Isotopes for Glacial Ocean Conditions, Use Proxies Paleoceanogr. Examples from South Atl., 513–522, 1999.

Lenton, T. M., Williamson, M. S., Edwards, N. R., Marsh, R., Price, A. R., Ridgwell, A. J., Shepherd, J. G. and Cox, S. J.: Millennial timescale carbon cycle and climate change in an efficient Earth system model, Clim. Dyn., 26(7–8), 687–711, doi:10.1007/s00382-006-0109-9, 2006.

Lenton, T. M., Marsh, R., Price, A. R., Lunt, D. J., Aksenov, Y., Annan, J. D., Cooper-Chadwick, T., Cox, S. J., Edwards, N. R., Goswami, S., Hargreaves, J. C., Harris, P. P., Jiao, Z., Livina, V. N., Payne, A. J., Rutt, I. C., Shepherd, J. G., Valdes, P.

J., Williams, G., Williamson, M. S. and Yool, A.: Effects of atmospheric dynamics and ocean resolution on bi-stability of the thermohaline circulation examined using the Grid ENabled Integrated Earth system modelling (GENIE) framework, Clim. Dyn., 29(6), 591–613, doi:10.1007/s00382-007-0254-9, 2007.

Lippold, J., Luo, Y., Francois, R., Allen, S. E., Gherardi, J., Pichat, S., Hickey, B. and Schulz, H.: Strength and geometry of the glacial Atlantic Meridional Overturning Circulation, Nat. Geosci., 5(11), 813–816, doi:10.1038/ngeo1608, 2012.

Lund, D. C., Mix, A. C. and Southon, J.: Increased ventilation age of the deep northeast Pacific Ocean during the last deglaciation, Nat. Geosci., 4(11), 771–774, doi:10.1038/ngeo1272, 2011.

Lupker, M., France-Lanord, C., Galy, V., Lavé, J. and Kudrass, H.: Increasing chemical weathering in the Himalayan system since the Last Glacial Maximum, Earth Planet. Sci. Lett., 365, 243–252, doi:10.1016/j.epsl.2013.01.038, 2013.

Lynch-Stieglitz, J., Adkins, J. F., Curry, W. B., Dokken, T., Hall, I. R., Herguera, J. C., Hirschi, J. J.-M., Ivanova, E. V, Kissel, C., Marchal, O., Marchitto, T. M., McCave, I. N., McManus, J. F., Mulitza, S., Ninnemann, U., Peeters, F., Yu, E.-F. and Zahn, R.: Atlantic meridional overturning circulation during the Last Glacial Maximum., Science, 316(5821), 66–69, doi:10.1126/science.1137127, 2007.

Ma, W. and Tian, J.: Modeling the contribution of dissolved organic carbon to carbon sequestration during the last glacial maximum, Geo-Marine Lett., 34(5), doi:10.1007/s00367-014-0378-y, 2014.

Mahowald, N. M., Muhs, D. R., Levis, S., Rasch, P. J., Yoshioka, M., Zender, C. S. and Luo, C.: Change in atmospheric mineral aerosols in response to climate: Last glacial period, preindustrial, modern, and doubled carbon dioxide climates, J. Geophys. Res. Atmos., 111(10), doi:10.1029/2005JD006653, 2006.

Marcott, S. A., Bauska, T. K., Buizert, C., Steig, E. J., Rosen, J. L., Cuffey, K. M., Fudge, T. J., Severinghaus, J. P., Ahn, J., Kalk, M. L., McConnell, J. R., Sowers, T., Taylor, K. C., White, J. W. C. and Brook, E. J.: Centennial-scale changes in the global carbon cycle during the last deglaciation, Nature, 514(7524), 616–619, doi:10.1038/nature13799, 2014.

Marsh, R., Muller, S. A., Yool, A., and Edwards, N. R.: Incorporation of the C-GOLDSTEIN efficient climate model into the GENIE framework: “eb go gs” configurations of GENIE, Geosci. Model Dev., 4, 957–992, doi:10.5194/gmd-4-957-2011, 2011.

Martin, P., Archer, D. and Lea, D. W.: Role of deep sea temperature in the carbon cycle during the last glacial, Paleoceanography, 20(2), 1–10, doi:10.1029/2003PA000914, 2005.

Martinez-Garcia, A., Sigman, D. M., Ren, H., Anderson, R. F., Straub, M., Hodell, D. A., Jaccard, S. L., Eglinton, T. I. and Haug, G. H.: Iron Fertilization of the Subantarctic Ocean During the Last Ice Age, Science, 343(6177), 1347–1350, doi:10.1126/science.1246848, 2014.

Masson-Delmotte, V., Kageyama, M., Braconnot, P., Charbit, S., Krinner, G., Ritz, C., Guilyardi, E., Jouzel, J., Abe-Ouchi, A., Crucifix, M., Gladstone, R. M., Hewitt, C. D., Kitoh, A., LeGrande, A. N., Marti, O., Merkel, U., Motoi, T., Ohgaito, R., Otto-Bliesner, B., Peltier, W. R., Ross, I., Valdes, P. J., Vettoretti, G., Weber, S. L., Wolk, F. and Yu, Y.: Past and future polar amplification of climate change: Climate model intercomparisons and ice-core constraints, Clim. Dyn., 26(5), 513–529, doi:10.1007/s00382-005-0081-9, 2006.

Matsumoto, K., Sarmiento, J. L. and Brzezinski, M. A.: Silicic acid leakage from the Southern Ocean: A possible explanation for glacial atmospheric p CO $_2$, Global Biogeochem. Cycles, 16(3), 5-1-5–23, doi:10.1029/2001GB001442, 2002.

Matsumoto, K., Hashioka, T. and Yamanaka, Y.: Effect of temperature-dependent organic carbon decay on atmospheric pCO2, J. Geophys. Res. Biogeosciences, 112(2), doi:10.1029/2006JG000187, 2007.

Matsumoto, K., Tokos, K., Huston, A. and Joy-Warren, H.: MESMO 2: A mechanistic marine silica cycle and coupling to a simple terrestrial scheme, Geosci. Model Dev., 6(2), 477–494, doi:10.5194/gmd-6-477-2013, 2013.

Matsumoto, K., Chase, Z. and Kohfeld, K.: Different mechanisms of silicic acid leakage and their biogeochemical consequences, Paleoceanography, 29(3), 238–254, doi:10.1002/2013PA002588, 2014.

Menviel, L., Joos, F. and Ritz, S. P.: Simulating atmospheric CO 2, 13C and the marine carbon cycle during the Last Glacial-Interglacial cycle: Possible role for a deepening of the mean remineralization depth and an increase in the oceanic nutrient inventory, Quat. Sci. Rev., 56, 46–68, doi:10.1016/j.quascirev.2012.09.012, 2012.

Menviel, L., Mouchet, A., Meissner, K. J., Joos, F. and England, M. H.: Impact of oceanic circulation changes on atmospheric δ13CO2, Global Biogeochem. Cycles, 29(11), 1944–1961, doi:10.1002/2015GB005207, 2015.

Muglia, J. and Schmittner, A.: Glacial Atlantic overturning increased by wind stress in climate models, Geophys. Res. Lett., 42(22), 9862–9869, doi:10.1002/2015GL064583, 2015.

Munhoven, G.: Glacial - Interglacial changes of continental weathering: Estimates of the related CO2 and HCO3- flux variations and their uncertainties, Glob. Planet. Change, 33(1–2), 155–176, doi:10.1016/S0921-8181(02)00068-1, 2002.

O’Ishi, R. and Abe-Ouchi, A.: Influence of dynamic vegetation on climate change and terrestrial carbon storage in the Last Glacial Maximum, Clim. Past, 9(4), 1571–1587, doi:10.5194/cp-9-1571-2013, 2013.

Oka, A., Abe-Ouchi, A., Chikamoto, M. O. and Ide, T.: Mechanisms controlling export production at the LGM: Effects of changes in oceanic physical fields and atmospheric dust deposition, Global Biogeochem. Cycles, 25, doi:10.1029/2009GB003628, 2011.

Opdyke, B. N. and Walker, J. C. G.: Return of the coral reef hypothesis: basin to shelf partitioning of CaCO3 and its effect on atmospheric CO2, Geology, 20(8), 733–736, doi:10.1130/0091-7613(1992)020<0733:ROTCRH>2.3.CO, 1992.

Oppo, D. W., Curry, W. B. and McManus, J. F.: What do benthic δ13C and δ18O data tell us about Atlantic circulation during Heinrich Stadial 1?, Paleoceanography, 30(4), 353–368, doi:10.1002/2014PA002667, 2015.

Otto, D., Rasse, D., Kaplan, J., Warnant, P. and François, L.: Biospheric carbon stocks reconstructed at the Last Glacial Maximum: Comparison between general circulation models using prescribed and computed sea surface temperatures, Glob. Planet. Change, 33(1–2), 117–138, doi:10.1016/S0921-8181(02)00066-8, 2002.

Palastanga, V., Slomp, C. P. and Heinze, C.: Glacial-interglacial variability in ocean oxygen and phosphorus in a global biogeochemical model, Biogeosciences, 10(2), 945–958, doi:10.5194/bg-10-945-2013, 2013.

Peltier, W. R.: Ice age paleotopography., Science, 265(5169), 195–201, doi:10.1126/science.265.5169.195, 1994.

Peterson, C. D., Lisiecki, L. E. and Stern, J. V.: Deglacial whole-ocean δ13C change estimated from 480 benthic foraminiferal records, Paleoceanography, 29(6), 549–563, doi:10.1002/2013PA002552, 2014.

Prentice, I., Farquhar, G. and Fasham, M.: The carbon cycle and atmospheric carbon dioxide, Clim. Chang. 2001 Sci. Basis, 183–237, doi:10.1256/004316502320517344, 2001.

Prentice, I., Harrison, S. and Bartlein, P.: Global vegetation and terrestrial carbon cycle changes after the last ice age, New Phytol., 189(4), 988–998, doi:10.1111/j.1469-8137.2010.03620.x, 2011.

Radi, T. and de Vernal, A.: Last glacial maximum (LGM) primary productivity in the northern North Atlantic Ocean, Can. J. Earth Sci., 45, 1299–1316, doi:Doi 10.1139/E08-059, 2008.

Ridgwell, A. and Hargreaves, J. C.: Regulation of atmospheric CO2 by deep-sea sediments in an Earth system model, Global Biogeochem. Cycles, 21(2), doi:10.1029/2006GB002764, 2007.

Ridgwell, A., Hargreaves, J. C., Edwards, N. R., Annan, J. D., Lenton, T. M., Marsh, R., Yool, A. and Watson, A.: Marine geochemical data assimilation in an efficient Earth System Model of global biogeochemical cycling, Biogeosciences, 4(4), 87–104, doi:10.5194/bg-4-87-2007, 2007.

Roth, R., Ritz, S. P. and Joos, F.: Burial-nutrient feedbacks amplify the sensitivity of atmospheric carbon dioxide to changes in organic matter remineralisation, Earth Syst. Dyn., 5(2), 321–343, doi:10.5194/esd-5-321-2014, 2014.

Sarnthein, M., Schneider, B. and Grootes, P. M.: Peak glacial 14C ventilation ages suggest major draw-down of carbon into the abyssal ocean, Clim. Past, 9(6), 2595–2614, doi:10.5194/cp-9-2595-2013, 2013.

Schmitt, J., Schneider, R., Elsig, J., Leuenberger, D., Lourantou, A., Chappellaz, J., Kohler, P., Joos, F., Stocker, T. F., Leuenberger, M. and Fischer, H.: Carbon Isotope Constraints on the Deglacial CO2 Rise from Ice Cores, Science, 336(6082), 711–714, doi:10.1126/science.1217161, 2012.

Schmittner, A. and Somes, C. J.: Complementary constraints from carbon (13C) and nitrogen (15N) isotopes on the glacial ocean's soft-tissue biological pump, Paleoceanography, 31(6), 669–693, doi:10.1002/2015PA002905, 2016.

Schmittner, A., Urban, N. M., Shakun, J. D., Mahowald, N. M., Clark, P. U., Bartlein, P. J., Mix, A. C. and Rosell-Mele, A.: Climate Sensitivity Estimated from Temperature Reconstructions of the Last Glacial Maximum, Science (80-.)., 334(6061), 1385–1388, doi:10.1126/science.1203513, 2011.

Shin, S.-I., Liu, Z., Otto-Bliesner, B., Brady, E., Kutzbach, J. and Harrison, S.: A Simulation of the Last Glacial Maximum climate using the NCAR-CCSM, Clim. Dyn., 20(2), 127–151, doi:10.1007/s00382-002-0260-x, 2003.

Sigman, D. M. and Boyle, E. A.: Glacial/Interglacial Variations In Atmospheric Carbon Dioxide, Nature, 407(6806), 859–869, doi:10.1038/35038000, 2000.

Simmons, C. T., Mysak, L. A., and Matthews, H. D.: An investigation of carbon cycle dynamics since the Last Glacial Maximum: Complex interactions between the terrestrial biosphere, weathering, ocean alkalinity, and CO2 radiative warming in an Earth system model of intermediate complexity, Clim. Past Discuss., doi:10.5194/cp-2016-24, in review, 2016.

Singh, A. D., Jung, S. J. A., Darling, K., Ganeshram, R., Ivanochko, T. and Kroon, D.: Productivity collapses in the Arabian Sea during glacial cold phases, Paleoceanography, 26(3), doi:10.1029/2009PA001923, 2011.

Skinner, L. C., Fallon, S., Waelbroeck, C., Michel, E. and Barker, S.: Ventilation of the Deep Southern Ocean and Deglacial CO2 Rise, Science (80-.)., 328(5982), 1147–1151, doi:10.1126/science.1183627, 2010.

Skinner, L. C., Waelbroeck, C., Scrivner, A. E. and Fallon, S. J.: Radiocarbon evidence for alternating northern and southern sources of ventilation of the deep Atlantic carbon pool during the last deglaciation, Proc. Natl. Acad. Sci., 111(15), 5480–5484, doi:10.1073/pnas.1400668111, 2014.

Skinner, L., McCave, I. N., Carter, L., Fallon, S., Scrivner, A. E. and Primeau, F.: Reduced ventilation and enhanced magnitude of the deep Pacific carbon pool during the last glacial period, Earth Planet. Sci. Lett., 411, 45–52, doi:10.1016/j.epsl.2014.11.024, 2015.

Smith, H. J., Fischer, H., Wahlen, M., Mastroianni, D. and Deck, B.: Dual modes of the carbon cycle since the Last Glacial Maximum, Nature, 400(6741), 248–250, doi:10.1038/22291, 1999.

Stephens, B. B. and Keeling, R. F.: The influence of antarctic sea ice on glacial-interglacial CO2 variations, Nature, 404(6774), 171–174, doi:10.1038/35004556, 2000.

Sun, X. and Matsumoto, K.: Effects of sea ice on atmospheric p CO 2 : A revised view and implications for glacial and future climates, J. Geophys. Res., 115(G2), 1–8, doi:10.1029/2009JG001023, 2010.

Tamburini, F. and Föllmi, K. B.: Phosphorus burial in the ocean over glacial-interglacial time scales, Biogeosciences, 6(4), 501–513, doi:10.5194/bg-6-501-2009, 2009.

Tiedemann, R. , Ronge, T. , Lamy, F. , Köhler, P. , Frische, M. , De Pol Holz, R. , Pahnke, K., Alloway, B. V. , Wacker, L. and Southon, J.: New Constraints on the Glacial Extent of the Pacific Carbon Pool and its Deglacial Outgassing , Nova Act Lc, 121 (408), 229-233, 2015.

Toggweiler, J. R., Russell, J. L. and Carson, S. R.: Midlatitude westerlies, atmospheric CO2, and climate change during the ice ages, Paleoceanography, 21(2), doi:10.1029/2005PA001154, 2006.

Tréguer, P. and Pondaven, P.:Global change: Silica control of carbon dioxide, Nature, 486, 358–359, 2000.

Vance, D., Teagle, D. A. H. and Foster, G. L.: Variable Quaternary chemical weathering fluxes and imbalances in marine geochemical budgets, Nature, 458(7237), 493–496, doi:10.1038/nature07828, 2009.

Völker, C. and Köhler, P.: Responses of ocean circulation and carbon cycle to changes in the position of the Southern Hemisphere westerlies at Last Glacial Maximum, Paleoceanography, 28(4), 726–739, doi:10.1002/2013PA002556, 2013.

Waelbroeck, C., Paul, A., Kucera, M., Rosell-Melé, A., Weinelt, M., Schneider, R., Mix, A. C., Abelmann, A., Armand, L., Bard, E., Barker, S., Barrows, T. T., Benway, H., Cacho, I., Chen, M. T., Cortijo, E., Crosta, X., De Vernal, A., Dokken, T., Duprat, J., Elderfield, H., Eynaud, F., Gersonde, R., Hayes, A., Henry, M., Hillaire-Marcel, C., Huang, C. C., Jansen, E., Juggins, S., Kallel, N., Kiefer, T., Kienast, M., Labeyrie, L., Leclaire, H., Londeix, L., Mangin, S., Matthiessen, J., Marret, F., Meland, M., Morey, A. E., Mulitza, S., Pflaumann, U., Pisias, N. G., Radi, T., Rochon, A., Rohling, E. J., Sbaffi, L., Schäfer-Neth, C., Solignac, S., Spero, H., Tachikawa, K. and Turon, J. L.: Constraints on the magnitude and patterns of ocean cooling at the Last Glacial Maximum, Nat. Geosci., 2(2), 127–132, doi:10.1038/ngeo411, 2009.

Wagner, M. and Hendy, I. L.: Trace metal evidence for a poorly ventilated glacial Southern Ocean, Clim. Past Discuss., https://doi.org/10.5194/cpd-11-637-2015, 2015.

Wallmann, K.: Is late Quaternary climate change governed by self-sustained oscillations in atmospheric CO2?, Geochim. Cosmochim. Acta, 132, 413–439, doi:10.1016/j.gca.2013.10.046, 2014.

Wallmann, A.: Effects of Eustatic Sea-Level Change on Atmospheric CO_2 and Glacial Climate. Nova Act Lc NF, 121, 241-245, 2015.

Watson, A. J. and Naveira Garabato, A. C.: The role of Southern Ocean mixing and upwelling in glacial-interglacial atmospheric CO2change, Tellus, Ser. B Chem. Phys. Meteorol., 58(1), 73–87, doi:10.1111/j.1600-0889.2005.00167.x, 2006.

Weber, S. L., Drijfhout, S. S., Abe-Ouchi, A., Crucifix, M., Eby, M., Ganopolski, A., Murakami, S., Otto-Bliesner, B., and Peltier, W. R.: The modern and glacial overturning circulation in the Atlantic ocean in PMIP coupled model simulations, Clim. Past, 3, 51-64, https://doi.org/10.5194/cp-3-51-2007, 2007.

Weitemeyer, K. A. and Buffett, B. A.: Accumulation and release of methane from clathrates below the Laurentide and Cordilleran ice sheets, Global Planet Change, 53(3), 176–187, 2006.

Williamson, M. S., Lenton, T. M., Shepherd, J. G. and Edwards, N. R.: An efficient numerical terrestrial scheme (ENTS) for Earth system modelling, Ecol. Modell., 198(3–4), 362–374, doi:10.1016/j.ecolmodel.2006.05.027, 2006.

Yu, J., Anderson, R. and Rohling, E.: Deep Ocean Carbonate Chemistry and Glacial-Interglacial Atmospheric CO2 Change, Oceanography, 27(1), 16–25, doi:10.5670/oceanog.2014.04, 2014.

Zech, R.: A permafrost glacial hypothesis – Permafrost carbon might help explaining the Pleistocene ice ages, Quat. Sci. J., 61(1), 84–92, doi:10.3285/eg.61.1.07, 2012.

Zech, R., Huang, Y., Zech, M., Tarozo, R., and Zech, W.: High carbon sequestration in Siberian permafrost loess-paleosols during glacials, Clim. Past, 7, 501-509, doi:10.5194/cp-7-501-2011, 2011.

Zeng, N.: Glacial-interglacial atmospheric CO2 changes – the Glacial Burial Hypothesis. – Advances in Atmospheric Sciences, 20: 677–693, 2003.

Zeng, N.: Quasi-100 ky glacial-interglacial cycles triggered by subglacial burial carbon release, Clim. Past, 3, 135–153, doi:10.5194/cpd-2-371-2006, 2007.

Zhang, X., Lohmann, G., Knorr, G., and Xu, X.: Different ocean states and transient characteristics in Last Glacial Maximum simulations and implications for deglaciation, Clim. Past, 9, 2319-2333, doi:10.5194/cp-9-2319-2013, 2013.

Ziegler, M., Diz, P., Hall, I. R. and Zahn, R.: Millennial-scale changes in atmospheric CO2 levels linked to the Southern Ocean carbon isotope gradient and dust flux, Nat. Geosci., 6, 457–461, 2013.

Zimov, S., Schuur, E. and III, F. C.: Permafrost and the global carbon budget, Science, 312(June), 1612–1613, doi:10.1126/science.1128908, 2006.

Zimov, N. S., Zimov, S. A., Zimova, A. E., Zimova, G. M., Chuprynin, V. I., and Chapin, F. S.: Carbon storage in permafrost and soils of the mammoth tundra-steppe biome: Role in the global carbon budget, Geophys. Res. Lett., 36, L02502, doi:10.1029/2008gl036332, 2009.